ACS Catalysis

pubs.acs.org/acscatalysis
Research Article

Lifecycle of Pd Clusters: Following the Formation and Evolution of Active Pd Clusters on Ceria During CO Oxidation by In Situ/Operando Characterization Techniques

Daria Gashnikova, Florian Maurer, Miriam R. Bauer, Sarah Bernart, Jelena Jelic, Mads Lützen, Carina B. Maliakkal, Paolo Dolcet, Felix Studt, Christian Kübel, Christian D. Damsgaard, Maria Casapu, and Jan-Dierk Grunwaldt*

Cite This: ACS Catal. 2024, 14, 14871−14886
Read Online

ACCESS | Metrics & More | Article Recommendations | Supporting Information

ABSTRACT: For maximizing the atomic efficiency in noble metal-based catalysts, dedicated preparation routes and high lifetime are essential. Both aspects require an in-depth understanding of the fate of noble metal atoms under reaction conditions. For this purpose, we used a combination of complementary *in situ/operando* characterization techniques to follow the lifecycle of the Pd sites in a 0.5% Pd/5% CeO_2−Al_2O_3 catalyst during oxygen-rich CO oxidation. Time-resolved X-ray absorption spectroscopy showed that Pd cluster formation under reaction conditions is important for a high CO oxidation activity. In combination with density functional theory calculations, we concluded that the ideal Pd cluster size amounts to about 10−30 Pd atoms. The cluster formation and stability were affected by the applied temperature and reaction conditions. Already short pulses of 1000 ppm CO in the lean reaction feed were found to trigger sintering of Pd at temperatures below 200 °C, while at higher temperatures oxidation processes prevailed. Environmental transmission electron microscopy unraveled redispersion at higher temperatures (400−500 °C) in oxygen atmosphere, leading to the formation of single sites and thus the loss of activity. However, due to the reductive nature of CO, clusters formed again upon cooling in reaction atmosphere, thus closing the catalytic cycle. Exploiting the gained knowledge on the lifecycle of Pd clusters, we systematically investigated the effect of catalyst composition on the cluster formation tendency. As uncovered by DRIFTS measurements, the Pd to CeO_2 ratio seems to be a key descriptor for Pd agglomeration under reaction conditions. While for higher Pd loadings, the probability of cluster formation increased, a higher CeO_2 content leads to the formation of oxidized dispersed Pd species. According to our results, a Pd:CeO_2 weight ratio of 1:10 for CeO_2−Al_2O_3-supported catalysts leads to the highest CO oxidation activity under lean conditions independent of the applied synthesis method.

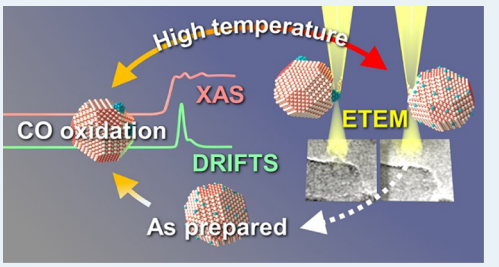

KEYWORDS: *in situ/operando characterization, palladium−ceria, cluster formation, catalytic lifecycle, CO oxidation*

1. INTRODUCTION

Noble metal single atoms, clusters, and nanoparticles deposited on metal oxide supports are prominent catalytic materials in several areas such as electrocatalysis,[1−3] green energy and fuel production,[4,5] and environmental catalysis.[6−9] These processes play a significant role in the development of more sustainable technologies and emission reduction for clean air. The viability of such catalytic processes is directly linked to the maximum efficiency of the noble metals.[4,10,11] In this respect, single atom catalysts have been proposed to have the highest efficiency, but various *in situ* and *operando* studies have shown that (a) the catalyst changes strongly under reaction conditions,[12,13] (b) clusters and/or particles are more active,[14,15] and (c) the support plays a decisive role.[16] Considering that for any catalytic application the identification of the nature of the most active species is essential for a rational catalyst design, a fundamental understanding of the catalyst lifecycle, including the *in situ* formation of active centers, and of the possible activation/deactivation processes on an atomic scale is mandatory.

In recent years, numerous research efforts have been undertaken to investigate the dependence of the oxidation activity on the noble metal entity size for CeO_2-supported catalysts. CeO_2 represents a well-suited support since it stabilizes the noble metal and prevents its sintering at higher temperatures. However, under oxidizing conditions and at elevated temperatures, the formation of atomically dispersed species was observed,[17] which for Pt/CeO_2-based catalysts was found to be disadvantageous during CO oxidation. With the

Received: April 8, 2024
Revised: August 22, 2024
Accepted: August 29, 2024
Published: September 23, 2024

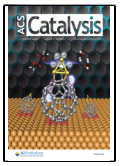

Table 1. Overview of Investigated Samples, Their Preparation, and Sample Acronyms Used in the Manuscript

Sample acronym	Sample composition	Synthesis method
0.25Pd 5CeAl-FSP	0.25% Pd/5% CeO_2−Al_2O_3	double-nozzle flame spray pyrolysis, CeO_2 and Al_2O_3 precursors in one solution
0.5Pd 5CeAl-FSP	0.5% Pd/5% CeO_2−Al_2O_3	double-nozzle flame spray pyrolysis
1.0Pd 5CeAl-FSP	1.0% Pd/5% CeO_2−Al_2O_3	double-nozzle flame spray pyrolysis
0.5Pd 10CeAl-FSP	0.5% Pd/10% CeO_2−Al_2O_3	double-nozzle flame spray pyrolysis
0.5Pd 20CeAl-FSP	0.5% Pd/20% CeO_2−Al_2O_3	double-nozzle flame spray pyrolysis
0.5PdAl 5Ce-FSP	0.5% Pd/5% CeO_2−Al_2O_3	double-nozzle flame spray pyrolysis, Pd and Al_2O_3 precursors in one solution
0.5Pd 5CeAl-IWI	0.5% Pd/5% CeO_2−Al_2O_3	incipient wetness impregnation
0.5Pd 10CeAl-IWI	0.5% Pd/10% CeO_2−Al_2O_3	incipient wetness impregnation
1.0Pd/CeO_2-FSP	1.0% Pd/CeO_2	single-nozzle flame spray pyrolysis
1.0Pd/CeO_2-LSA	1.0% Pd/CeO_2	incipient wetness impregnation of low-surface-area (LSA) CeO_2

help of comprehensive *operando* characterization in combination with theoretical calculations, reduced Pt clusters in the size range of 1−2 nm were identified to be particularly active in CO oxidation for the Pt/CeO_2 system.[18−21] Moreover, it was shown that the size of the Pt particles can be tuned by applying reductive pulses, enabling the reactivation of redispersed catalysts.[22] In addition, the cluster formation tendency can be enhanced by the adjustment of the surface noble metal concentration (SNMC),[23] e.g., by increasing the noble metal loading.

Despite the fact that there are also several studies related to Pd/CeO_2 catalysts, their active states during CO oxidation are controversially debated. In the literature, Pd single sites,[24−26] clusters,[27,28] or even particles[29] are reported to be the active species for CO oxidation. However, the direct comparison of the results is often challenging, due to different catalyst preparation methods, activation procedures, testing conditions, noble metal loadings, or specific surface areas of the used CeO_2 carrier. Despite similar as-prepared states and identical noble metal loadings are applied, catalysts can differ strongly with respect to their tendency to form clusters under reaction conditions, since this process depends heavily on the applied gas mixture and surface noble metal concentration.[23,30] In particular, a stronger reduction/sintering of noble metal species and partial reduction of the CeO_2 surface are expected to occur in reaction mixtures with high CO concentration and lower oxygen content in comparison to oxygen-rich conditions. On the contrary, in case of lean reaction conditions, the formation of inactive single atom sites is a challenge.[19] In their recent work, Muravev et al.[31] highlighted the role of CeO_2 crystallite size in the CO oxidation activity of Pd-based catalysts. According to their findings, a smaller size of CeO_2 nanocrystals improves the stability of highly dispersed noble metal species under CO-rich reaction conditions due to the higher oxygen mobility of the support nanoparticles. These results underline that an intelligent support design allows for the stabilization of the desired noble metal species during the reaction. Finally, the use of combined supports may improve the durability of the catalyst due to strong noble metal−support interactions between Pt and CeO_2, as, for example, reported by Li et al.[32] and Xie et al.[33] for the Pt/CeO_x/SiO_2 and Pt/CeO_2−Al_2O_3 systems, respectively.

In order to identify the structures of Pt- and Pd-based catalysts under reaction conditions, *operando* techniques are decisive,[34,35] and X-ray absorption spectroscopy (XAS) is an ideal tool.[36] This characterization technique is element-specific and bulk-sensitive and provides information on the local structure and electronic state of the noble metal during operation.[11] On the other hand, the use of complementary diffuse reflectance infrared Fourier transform spectroscopy (DRIFTS) enables selective probing of the catalyst surface.[37] Combined with density functional theory (DFT) calculations, such an approach provides possibilities for determining the noble metal structure and allows interlinking with complementary spectroscopic data.[19,24,38] Moreover, with the developments in the field of electron microscopy, *in situ* transmission electron microscopy (TEM) becomes a powerful tool for the visualization of local structural changes under a reactive atmosphere,[39] thus leading to a holistic picture on the noble metal state.

In this study, we aim to follow the lifecycle of active Pd species under dynamic CO oxidation conditions in a high excess of oxygen, which is typical for many air purification applications, by means of complementary *in situ/operando* characterization techniques. A combination of *operando* XAS and DRIFTS in conjunction with DFT calculations was used for the identification of the active Pd state and determination of the optimal cluster size range. The tendency toward the formation of Pd clusters and single sites was investigated as a function of temperature and reaction conditions during reduction−oxidation switching experiments using time-resolved XAS. Furthermore, the stability of formed Pd clusters under oxidizing atmosphere was evaluated by environmental transmission electron microscopy (ETEM). Finally, the effect of catalyst composition on the cluster formation tendency and therefore on the catalytic activity has been systematically studied. In this way, we aim at obtaining a correlation between the observed activity, cluster size, and catalyst composition and at monitoring the cluster evolution under reaction conditions.

2. MATERIALS AND METHODS

2.1. Catalyst Preparation. The Pd-based catalysts were synthesized by flame spray pyrolysis (FSP) using an in-house built setup, which is described in more detail in ref[40−42]. Depending on the desired noble metal/ceria weight ratio, the corresponding amounts of palladium acetylacetonate (ACROS Organics, 35% Pd) and ceria ethylhexanoate (Alfa Aesar, 12% Ce) were dissolved in 250 mL xylene and sprayed separately from the solution containing the alumina precursor. For the 0.5% Pd/5% CeO_2−Al_2O_3 sample, 47.4 mg palladium acetylacetonate and 1.12 g cerium ethylhexanoate together with 19.9 g aluminum acetylacetonate were used. Due to the low solubility of aluminum acetylacetonate (Sigma-Aldrich, ≥98%) in xylene, a mixture of acetic acid and methanol with a volume ratio of 1:1 was used. The total precursor concentration was always fixed to 0.125 M. An overview on the synthesized samples is given in Table 1.

https://doi.org/10.1021/acscatal.4c02077
ACS Catal. 2024, 14, 14871−14886

The FSP setup was located in a well-ventilated fume cupboard and was used in a double-nozzle configuration.[41,42] The solutions were dosed via capillary tubes with a flow of 5 mL/min and dispersed with an O_2 flow of 5 L/min at a back pressure of 3 bar. The two nozzles were positioned at an angle of 120°, and the distance between the nozzles was fixed to 10.6 cm. The ignition of the sprays took place in an annular CH_4 flame (0.75 L/min CH_4 and 1.6 L/min O_2). The gas flows were adjusted by mass flow controllers (Bronkhorst). The formed nanoparticles were collected on water-cooled glass fiber filters (Glasfaser Filter GF 6, Whatman) placed in a cylindrical filter holder connected to a vacuum pump. The catalyst powder was collected from the filters and calcined at 500 °C for 5 h in static air in order to remove the remaining precursor residues.

Additionally, several Pd catalysts were prepared via incipient wetness impregnation using the following synthetic procedure: prior to the synthesis, γ-Al_2O_3 (Puralox, Sasol) was calcined in static air at 700 °C for 5 h. In the first step, γ-Al_2O_3 (pore volume 0.5 mL/g) was impregnated with a solution of cerium(III)-nitrate hexahydrate (Alfa Aesar, 99.99%). For the 5 or 10 wt % CeO_2−Al_2O_3 support, the corresponding amount of the cerium precursor was dissolved in water and added to the commercial Al_2O_3 support. In the case of the 10 wt % CeO_2−Al_2O_3 support, the cerium precursor solution was added to Al_2O_3 in two steps, with the powder being dried in-between at 70 °C for 1 h. After the addition of the precursor solution, both impregnated supports were dried at 70 °C for 1 h and subsequently calcined in air at 500 °C for 5 h. Next, the corresponding amount of tetraamminepalladium(II) nitrate solution (abcr, 5.0% Pd) in water was added dropwise to the obtained CeO_2−Al_2O_3 support. In an analogous manner, the catalysts were dried at 70 °C for 1 h and calcined in air at 500 °C for 5 h. For the 1.0 wt % Pd/CeO_2 sample, the Pd precursor solution was added in two steps to the commercial CeO_2 support (pore volume 0.1 mL/g). The dried catalyst was calcined at 500 °C for 5 h.

2.2. Catalytic Tests. For the CO oxidation tests, 100 mg of the catalyst (sieve fraction 125−250 μm) was diluted with 900 mg of quartz (Sigma-Aldrich, washed and calcined for analysis) and placed in a tubular quartz reactor with an inner diameter of 8 mm. The total gas flow was set to 500 mL/min to obtain a weight hourly space velocity (WHSV) of 300 L/(g_{cat} h) or 60 000 L/($g_{noble\ metal}$ h). The amount of the catalyst, dilution, and the total gas flow were adjusted to the noble metal loading, keeping an overall reactor loading of 1 g. The temperature inside the reactor was monitored by two thermocouples placed upstream and downstream of the catalyst bed. The gas composition at the reactor outlet was continuously analyzed using an online Fourier transform infrared spectrometer (Multigas 2030 FTIR Continuous Gas Analyzer, MKS Instruments).

For the evaluation of the catalytic activity, the catalyst was heated up to 500 °C at 5 K/min in a mixture of 1000 ppm CO, 8 vol % O_2, and N_2 as balance. The temperature was held for 1 h before the catalyst was cooled to room temperature. The gas flows were adjusted via mass flow controllers (Bronkhorst). To evaluate the catalyst stability, three consecutive cycles were performed between room temperature and 500 °C.

2.3. *Ex situ* Characterization. Elemental composition of the samples and palladium loading were determined by inductively coupled plasma optical emission spectroscopy (ICP-OES) using an iCAP 7600 DUO (Thermo Fisher Scientific) at the Institute for Applied Materials (IAM-AWP) at the Karlsruhe Institute for Technology (KIT). Prior to the elemental analysis, the samples were digested using acids and the pressure digestion system DAB-2.

The specific surface area was determined by N_2 physisorption according to the Brunauer−Emmett−Teller[43] (BET) method on the BELSORP-mini II (BEL Inc.). Depending on the sample, 30−40 points were recorded during the adsorption experiments. On average, around 10 measuring points were located in the BET region. Prior to analysis, the samples were degassed under reduced pressure at 300 °C for 2 h.

Powder X-ray diffraction (XRD) patterns were recorded by using a Bruker Advance D8 diffractometer with nickel-filtered CuKα radiation (wavelength = 0.154 nm) in the 2θ range between 10 and 120° with a step size of 0.016° and an acquisition time of 3 s per point.

High angle annular dark field scanning transmission electron microscopy (HAADF-STEM) images and energy dispersive X-ray spectroscopy (EDXS) mappings were acquired with a FEI Themis Z or FEI Themis 300 electron microscope operated at 300 keV at the Institute of Nanotechnology at KIT. The samples were deposited in a dry state on a carbon-supported copper grid. Prior to the deposition, the TEM grids were plasma-cleaned 2 times for 30 s at 50% device power (1070 NanoClean, Fischione Instruments).

Ex situ X-ray absorption spectroscopy (XAS) measurements were performed at the Pd K-edge. Prior to the measurements, the samples were diluted with cellulose and pressed into pellets. The XAS spectra were recorded in transmission mode at the CAT-ACT beamline[44] of the KIT light source for the following samples: 0.5Pd 5CeAl-FSP, 0.5Pd 10CeAl-FSP, 1.0Pd CeO_2-FSP, and 1.0Pd CeO_2-LSA. For tuning the energy of the incident X-ray beam, a double crystal monochromator (DCM) with Si(311)-oriented crystals was used. The size of the X-ray beam was set to 3.0 × 3.0 mm. Due to time limitations, the *ex situ* XAS measurements of the remaining samples were performed at the SAMBA beamline of the synchrotron radiation facility SOLEIL (Si(220)-DCM; beam size of 0.2 mm in height and 1.5 mm in width) and the P65 beamline of the synchrotron radiation facility DESY (Si(311)-DCM; beam size of 0.3 mm in height and 1.35 mm in width).

2.4. *Operando* XAS Characterization. *Operando* XAS measurements were conducted at the beamline ROCK[45] of the synchrotron radiation facility SOLEIL (Saint-Aubin, France) using Si(111) channel-cut crystal for monochromatization with an excenter disk.[46] Two different protocols were used to elucidate the catalyst state during transient light-off/light-out cycles and during rapid switches of the gas composition. For all *in situ/operando* investigations, few milligrams (5.0 mg or 7.0 mg) of the sieved catalyst powder (100−200 μm) were loaded in a capillary microreactor (1.5 mm outer diameter, 0.01 mm wall thickness). Gases were supplied via mass flow controllers (Bronkhorst). The total gas flow was set to 50 or 70 mL/min, yielding a WHSV of 120 000 L/($g_{noble\ metal}$ h). The catalysts were heated and cooled at a ramp rate of 5 K/min using either a hot air blower (FMB Oxford)[47,48] or a high-temperature cell.[49] The gas concentration was monitored online at the reactor outlet using a mass spectrometer (Omnistar, Pfeiffer Vacuum) and a Fourier transform infrared spectrometer (Multigas 2030 FTIR Continuous Gas Analyzer, MKS Instruments).

https://doi.org/10.1021/acscatal.4c02077
ACS Catal. 2024, 14, 14871−14886

During the CO oxidation light-off/light-out experiments, the *operando* XAS spectra at the Pd K-edge were recorded in fluorescence mode using a PIPS (Passivated Implanted Planar Silicon) fluorescence detector. The size of the beam was set to 0.3 mm in height and 0.5 mm in width. A light-off/light-out cycle involved the heating of the catalyst bed (0.5Pd 5CeAl-FSP) to 500 °C, without any pretreatment, at 5 K/min in reaction mixture (1000 ppm CO, 10 vol % O_2 and He) followed by cooling to room temperature after 1 h holding at 500 °C. The first cycle was considered a catalyst degreening run. During the second cycle, the catalyst was heated stepwise to 200 °C, while the extended X-ray absorption fine structure (EXAFS) spectra were collected with 2 Hz frequency in the middle of the catalyst bed for 30 min at each selected temperature. After reaching 200 °C, the sample was heated up to 500 °C at a heating rate of 5 K/min and was cooled to 50 °C after 1 h at 500 °C. To investigate the effect of the reductive treatment on the catalyst state evolution and performance, a 30 min reduction step was applied at 200 °C in 2% H_2/He followed by a catalytic cycle (0.5Pd 5CeAl-FSP-red200). During the latter cycle, EXAFS spectra were recorded at different temperatures below 200 °C before heating to 500 °C. Afterward, this procedure was repeated for the catalyst reduced for 30 min at 400 °C in 2% H_2/He, labeled 0.5Pd 5CeAl-FSP-red400.

The XAS data recorded at each temperature step were averaged to one single spectrum and normalized using a Python-based software developed at the SOLEIL synchrotron.[50] The EXAFS fitting of the experimental data in a k range of 2.5−13.9 $Å^{-1}$ was performed using the Artemis program from the IFFEFIT software package[51] in R space (1.1−3.4 Å using a multiple k weighting (k_w) = 1, 2, 3). For the EXAFS fitting of the experimental spectra with Pd cluster models of various sizes, aggregated FEFF calculations[52] were performed in the Artemis software for the determination of the merged cluster structures.

During rapid switches in the gas atmosphere (referred to as redox experiments), the *operando* XAS spectra were recorded at the Pd K-edge in transmission mode (beam size: 0.6 mm (in height) × 1.0 mm (in width)). The XAS spectra were recorded in the middle of the catalyst bed with a frequency of 1 Hz, resulting in 2 spectra per second. Prior to the switching experiments, two consecutive CO oxidation cycles were conducted from room temperature to 500 °C (heating and cooling rate: 10 K/min) to obtain a stable catalyst state. Based on the catalytic activity observed during the second light-off cycle, temperature points of different activity (25, 50, or 60% CO conversion) were selected for the gas mixture switching experiments (T25 = 63 °C, T50 = 87 °C, and T60 = 100 °C). At these temperatures, the reaction mixture was alternated between 1000 ppm CO/10% O_2/He and 10% O_2/He every 90 s for a total of 11 cycles. After completing the experiment at the selected temperatures and cooling to room temperature, two additional redox experiments were performed at 100 and 200 °C, but in this case, the reaction mixture was alternated between 1000 ppm CO/He and 10% O_2/He every 90 s for a total of 11 cycles.

The obtained XAS data were exported using the "Nexus extraction" software developed at the SOLEIL synchrotron.[50] The averaging, normalization, and LCA analysis of the recorded spectra in the energy range of 24 330−24 380 eV was performed using a Python script based on the Larch package.[53] The averaging over 10 spectra gave a time resolution of 5 s during cycling experiments. For the linear combination analysis (LCA), the spectra of the Pd foil and PdO references were recorded in transmission mode. For the estimation of the averaged fraction of oxidized Pd species, the LCA results of each cycle were summed up, divided by the number of performed cycles, and smoothed over 5 points to improve the signal-to-noise ratio. To obtain the noble metal oxidation and reduction rates at different temperatures, the first derivative of the smoothed average of the Pd_{ox} fraction was used.

2.5. Diffuse Reflectance Infrared Fourier Transform Spectroscopy (DRIFTS). Diffuse reflectance infrared Fourier transform spectroscopy (DRIFTS) measurements were performed on a VERTEX 70 Fourier transform infrared spectrometer (Bruker) equipped with Praying Mantis diffuse reflection optics (Harrick) and a liquid-nitrogen-cooled mercury cadmium telluride detector. For the DRIFTS measurements, the catalyst was diluted with CaF_2 (Thermo Scientific, 99.5%/Sigma-Aldrich, 99.99%) in a ratio of 1:4 and afterward pressed and sieved in the desired sieve fraction (100−200 μm). The temperature inside the cell was controlled by two heating cartridges located inside the cell and by a water-cooling system. Due to strong temperature gradients existing in the DRIFTS cell,[54] a correlation between the temperature set point and the actual temperature was estimated with an ImageIR 8300 camera (InfraTec).

Prior to the CO adsorption experiments, the catalysts were oxidatively pretreated at 350 °C for 1 h in 10% O_2/Ar. Afterward, the cell was stepwise cooled to the desired temperature (350 to 50 °C) where a background spectrum (4 cm^{-1} resolution; 100 spectra) was recorded for each temperature in 10% O_2/Ar at a gas flow of 200 mL/min. Subsequently, the DRIFTS experiments in the reaction mixture (1000 ppm CO/10% O_2/Ar, 200 mL/min) were performed. Afterward, the catalyst was heated in reaction mixture up to 350 °C. After 1 h at 350 °C, the catalyst was cooled in the reaction atmosphere to 30 °C and the catalytic cycle was repeated one more time. For the comparison of the different samples, the second cycle was selected. The gas composition at the cell outlet was constantly monitored using a mass spectrometer (Omnistar, Pfeiffer Vacuum). The background-corrected spectra (4 cm^{-1} resolution; 100 spectra) were converted to the Kubelka−Munk function by using the OPUS software (Bruker).

2.6. Environmental Transmission Electron Microscopy (ETEM). Environmental transmission electron microscopy (ETEM) measurements were conducted with a Cs aberration-corrected FEI-Titan ETEM (80−300 kV) electron microscope operated at 300 keV at the National Centre for Nano Fabrication and Characterization at the Technical University of Denmark (DTU Nanolab). The sample was suspended in high purity ethanol before deposition on a silicon nitride membrane through-hole chip (Wildfire, DENSsolutions). The gases were mixed via a gas mixing unit equipped with mass flow controllers and dosed via a needle valve and a pressure controller, which enabled accurate setting of gas pressure inside the microscope. Prior to the measurements, the sample holder and the Wildfire chip including the sample were cleaned in an O_2 plasma (Fischione Plasma Cleaner model 1020) to remove hydrocarbons. After inserting the holder into the microscope, the sample was oxidatively treated at 500 °C in 10 mbar O_2 for 1 h to remove the remaining adsorbates from the surface. After cooling, the sample was exposed to

https://doi.org/10.1021/acscatal.4c02077
ACS Catal. 2024, 14, 14871−14886

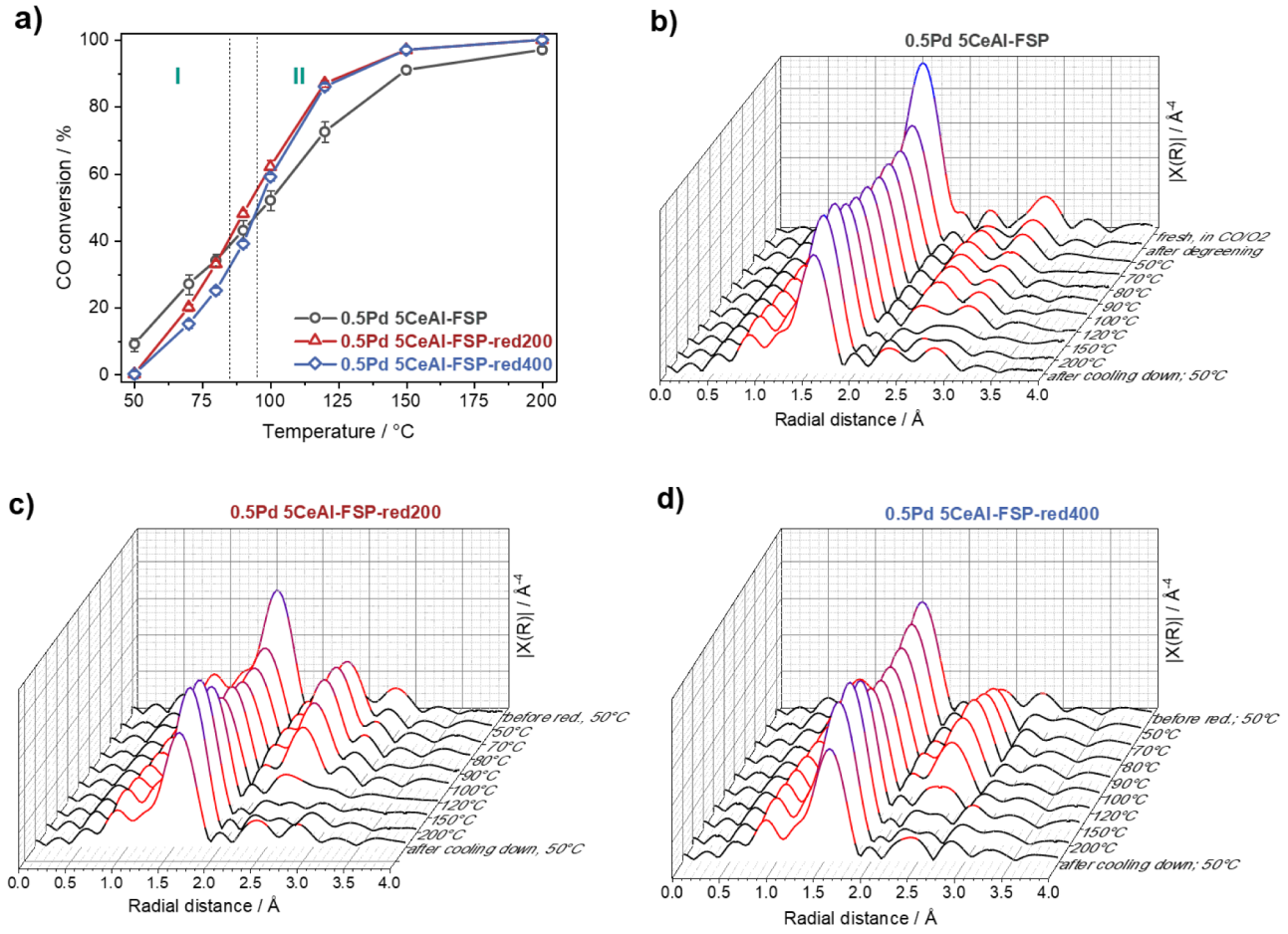

Figure 1. Catalytic activity results in terms of CO conversion (1000 ppm CO/10% O_2/He) of the 0.5Pd 5CeAl-FSP sample after degreening run (gray) and after reductive treatment in 2% H_2/He for 30 min at 200 °C (red) and 400 °C (blue). Above 90 °C (region II), a higher catalytic performance was observed after reductive treatment, while a higher activity is reached with the degreened catalyst in region I. Corresponding Fourier transform Pd K-edge EXAFS spectra (k^3-weigted, k-range: 2.5−13.9 Å^{-1}, not corrected for phase shift) of the 0.5Pd 5CeAl-FSP sample recorded in reaction mixture during the light-off cycle before (b) and after reductive treatment at 200 °C (c) and 400 °C (d).

reducing conditions (1.5 mbar H_2, gas flow 2 mL/min) and a heat treatment to 600 °C to initiate the formation of small clusters/nanoparticles. To be able to follow the redispersion process of Pd on CeO_2, the prereduced sample was heated to 500 °C in oxygen atmosphere (2.5 mbar O_2, gas flow 2 mL/min). The TEM images were taken under *operando* conditions (at high temperature in gas atmosphere) as well as at room temperature after rapid cooling (100−120 K/min). To minimize possible beam effects on the sample, the electron beam was blanked during the heating and cooling process. Moreover, the total electron dose rate was limited to 100 e/Å s to ensure the stability of the sample in the electron beam during the experiments.

2.7. Density Functional Theory Calculations. Density functional theory (DFT) calculations were performed using the Vienna Ab Initio Simulation Package (VASP)[55,56] in connection with the Atomic Simulation Environment (ASE).[57] All calculations used the projector augmented wave (PAW) method[58,59] and the Bayesian error estimation functional with van der Waals correlations (BEEF-vdW).[60]

2.7.1. Pd Cluster Models of Different Nuclearity. For calculations of reduced and partially oxidized Pd cluster models of various nuclearity, a plane-wave basis set with a cutoff energy of 400 eV was used. For a better description of localized Ce 4f electrons, the GGA+U (U = 5.0 eV) method[61] was applied. The optimized lattice constant of CeO_2 was 5.490 Å. Pd clusters with 3, 10, 19, and 30 Pd atoms were calculated on two-layer thick slabs of CeO_2(111) with 6 × 6 large unit cells, separated by 15 Å of vacuum in the z direction. During the geometry optimizations, the top layer of the CeO_2(111) surface as well as the Pd atoms and all adsorbates were allowed to relax while the bottom layer was kept fixed at the bulk position. The Brillouin zones were sampled using a (1 × 1 × 1) Monkhorst−Pack k-point grid.[62] The convergence criterion for geometry optimizations was a maximum force of 0.01 eV/Å. Spin polarization was considered in all calculations.

2.7.2. Diffusion Barriers of Pd_x (X = 1−3) on CeO_2. In order to follow the same procedure from our previous work on Pt_x diffusion,[20] structures used for Pd_x diffusion were calculated using slightly different parameters for the plane-wave cutoff (450 eV) and U (U = 5.0 eV) resulting in a lattice constant of 5.519 Å. Three layer-thick 3 × 3 large unit cells were used to represent CeO_2(111) infinite slab models, separated by more than 15 Å of vacuum in the z direction. All atoms in the top layer of the CeO_2(111) surface and the Pd atoms were allowed to relax during the geometry optimizations with the two bottom layers kept fixed at the bulk positions. The diffusion and aggregation barriers for the Pd_x systems were calculated using constrained optimizations in an analogous manner as for Pt/CeO_2(111) in our previous work (through calculating

https://doi.org/10.1021/acscatal.4c02077
ACS Catal. 2024, 14, 14871−14886

barrier heights by keeping one Pd−O bond distance fixed)[20] and climbing image nudged-elastic-band (CI-NEB) method.[63,64] The Brillouin zones were sampled using a (3 × 3 × 1) Monkhorst−Pack *k*-point grid.[62] The convergence criterion for geometry optimization was a maximum force of 0.01 eV/Å. Spin polarization was considered in all of the calculations.

3. RESULTS AND DISCUSSION

3.1. Dynamic Evolution of Pd Species Under Reaction Conditions. As described in Materials and Methods, flame spray pyrolysis (FSP) in a double-nozzle configuration was used to synthesize the 0.5% Pd/5% CeO_2−Al_2O_3 catalyst. During the synthesis, the Pd and CeO_2 precursors were sprayed in one flame, separately from the Al_2O_3 precursor, which allowed control of the location of the noble metal on ceria and achieving a close Pd−CeO_2 interaction. Due to the low contrast between Pd and CeO_2 and a high sensitivity of Pd to a long exposure to the electron beam as necessary for EDXS measurements, no assignment on the Pd particle size distribution was possible based on the electron microscopy data. However, HAADF-STEM and EDXS measurements of the as-prepared sample confirmed that Pd is located on CeO_2, which itself is distributed on the Al_2O_3 support (Figure S3c). Moreover, the low noble metal loading and the strong interaction with CeO_2 are expected to ensure the formation of highly dispersed Pd species, as it is demonstrated in the following by the *operando* XAS investigations. Due to the very dynamic nature of such systems, conventional methods for determining the noble metal particle size are unfortunately not suited, since such methods require a reductive pretreatment at high temperatures, leading to changes of the noble metal state and to significant noble metal sintering.

To study and follow the formation and evolution of active Pd species under reaction conditions, *operando* XAS spectra were stepwise-recorded during the CO oxidation light-off for the 0.5Pd 5CeAl-FSP sample. The influence of a reductive step on the oxidation activity and nature of Pd sites was evaluated during an analogous experiment after catalyst prereduction (200 and 400 °C). The catalytic activity data demonstrate a positive effect of the reductive treatment on the CO oxidation performance at temperatures above 90 °C (region II in Figure 1a). However, below 90 °C, the activity is slightly higher for the original (i.e., degreened) catalyst (region I in Figure 1a). According to the corresponding *operando* XAS data, Pd is in an oxidized state in the as-prepared sample, but the noble metal is partially reduced at the end of the degreening run. This is indicated by the decrease in Pd−O contribution at R = 1.5 Å (Figure 1b, data not corrected for phase shift) and the appearance of an additional feature at R = 2.5 Å in the FT-EXAFS spectra. This feature could not be mimicked by the EXAFS fitting of the experimental data with the DFT-calculated model of a single Pd atom located in four-fold hollow sites. On the contrary, the agreement with the experimental EXAFS data increased significantly after the implementation of Pd−Pd scattering from the Pd bulk model. The obtained results therefore demonstrate that the scattering path at R = 2.5 Å can be assigned to a Pd−Pd contribution, which suggests the *in situ* formation of small Pd clusters in addition to the Pd single sites. Further details on the fitting results can be found in Table S7 and Figure S11. In a first stage (up to 70 °C) during the CO oxidation light-off, the contribution of the scattering path at R = 2.5 Å becomes more pronounced while a further decrease in Pd−O scattering path is observed. These structural variations are caused by further catalyst reduction and noble metal cluster growth, both processes underlining the importance of few-atom Pd cluster formation for the low-temperature CO oxidation activity. At higher CO conversion (>50−60%), a partial reoxidation of Pd clusters occurs in the middle of the catalyst bed, which is suggested by the slight increase of the Pd−O backscattering contribution at 1.5 Å. Despite the possibility of EXAFS spectra recorded at higher temperatures being affected by thermal effects, e.g., thermal lattice vibrations, the same trends were observed in the evolution of the XANES spectra (Figure S8a).

After reduction at 200 °C in 2% H_2/He, larger Pd particles are formed, as indicated by the decreased Pd−O and more prominent Pd−Pd contributions in the FT-EXAFS spectrum, which was recorded after cooling in reaction mixture at 50 °C (Figure 1b). With respect to the catalyst evolution, the Pd clusters are further reduced during the CO oxidation light-off below 90 °C and partially reoxidized at higher temperatures, as also observed in the XANES spectra (Figure S8b). After the light-off/light-out cycle to 500 °C, the state of the prereduced catalyst is similar to the state observed for the degreened sample (Figure 1b vs Figure 1c). This suggests that a reoxidation/redispersion process takes place at higher temperatures during CO oxidation in lean atmosphere. A similar evolution is observed for the catalyst prereduced at 400 °C (Figures 1d and S8c). Interestingly, the contribution of the Pd−Pd coordination shell is lower after the reductive treatment at 400 °C than at 200 °C (Figure 1d). Taking into account that the cooling after the reductive treatment was performed in the lean reaction mixture, a stronger reoxidation/redispersion is expected in the O_2-containing atmosphere at these elevated temperatures.

The correlation of the activity results with the observed structural changes shows that the oxidized Pd clusters consisting of a small number of atoms appear to be the catalytically most active species at lower temperatures, while larger, more reduced Pd nanoparticles contribute to CO conversion at elevated temperatures. A decrease in the low-temperature activity after catalyst reduction most probably originates from the loss of noble metal−ceria interface sites due to the formation of larger Pd nanoparticles. As it was previously shown for the Pt/CeO_2 catalyst,[65] a slight reduction of the noble metal species is necessary for the formation of the activated interface state, while further sintering of noble metal particles leads to a decrease in the ceria reduction rate. The observed enhancement of the CO oxidation activity above 100 °C after catalyst reduction can be on the other hand explained by an improved adsorption of oxygen on the noble metal metallic-like sites with increasing temperature, as also reported by Muravev et al.[66] for Pd/CeO_2 and by Gänzler et al.[67] for Pt/CeO_2. Furthermore, the generation of slightly larger Pd nanoparticles during reduction in 2% H_2/He may slow down their full reoxidation and deactivation at T > 100 °C, as already observed for larger Pd nanoparticles.[68] As also demonstrated for the Pt/CeO_2 system,[22,69,70] the redispersion rate decreases with nanoparticle size, since larger noble metal nanoparticles are more difficult to oxidize and redisperse.

To estimate the size of Pd clusters after the reductive treatment at 200 °C and cooling in the reaction mixture, the fitting of the FT-EXAFS spectra was performed using DFT-calculated models of Pd clusters of various nuclearity (Pd_3, Pd_{10}, Pd_{19}, and Pd_{30}) supported on CeO_2(111) (Figure S9). Since the fit with only the Pd_3 cluster model could not

https://doi.org/10.1021/acscatal.4c02077
ACS Catal. 2024, 14, 14871−14886

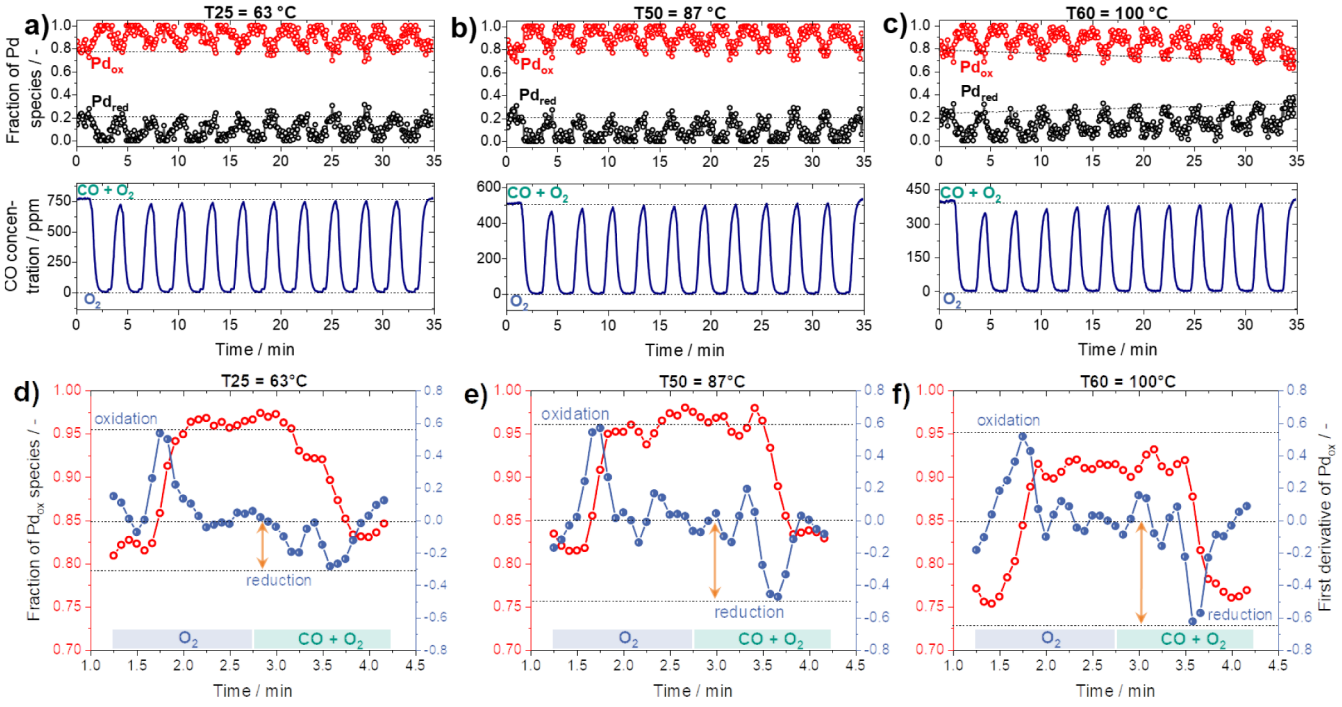

Figure 2. Linear combination results (LCA) of the Pd K-edge XANES spectra of 0.5Pd 5CeAl-FSP during switching experiments between 1000 ppm CO/10 O_2%/He and 10% O_2/He mixture at different light-off temperatures (T25 = 63 °C, T50 = 87 °C, and T60 = 100 °C) (a–c). The gas mixture was switched every 90 s during 11 cycles. The smoothed fraction of oxidized Pd species averaged over all cycles is additionally given for each temperature with the corresponding first derivative (d–f).

reproduce the first Pd–O coordination shell at 1.5 Å of the experimental spectrum (Table S11 and Figure S14b), a combination with a model representing single Pd atoms located at four-fold hollow sites on CeO_2 surfaces (e.g., CeO_2(110) PdO_2-sub) was necessary for a better fit with the experimental data. This suggests the coexistence of Pd clusters and single sites, which either did not agglomerate during the reductive treatment or partially redispersed again in the reaction mixture. According to the EXAFS analysis, the quality of the fit improved with increasing nuclearity of Pd clusters to Pd_{10}–Pd_{30} atoms (Table S12 and Figure S14c–f), with the Pd_{30} cluster model showing a slightly better fitting result. Note that the presence of surface-oxidized Pd clusters with a metallic core under lean reaction conditions cannot be excluded by means of XAS: oxide layers on the cluster surface may therefore also contribute to the Pd–O coordination shell observed at 1.5 Å (Table S13 and Figure S15). A similar trend in the EXAFS fitting results was also observed for the degreened 0.5Pd 5CeAl-FSP sample: as discussed above, the model of a single Pd atom was not able to reproduce the experimental spectrum and the presence of Pd agglomerates had to be considered despite their lower fraction (Table S7 and Figure S11). In line with the EXAFS analysis results observed for the reduced catalyst, the best agreement with the experimental data was observed for a combination of Pd single atom and Pd_{30} cluster models (Table S8 and Figure S12). Furthermore, the fitting of the experimental data was also possible using a combination of a Pd single atom and surface-oxidized $Pd_{30}O_n$ cluster models (Table S9 and Figure S13). Hence, according to the EXAFS analysis results and considering a certain particle size distribution, the formation of subnanometer Pd clusters (corresponding to 10–30 Pd atoms with an approximant size of ~0.7–0.8 nm) under reaction conditions was revealed for the 0.5Pd 5CeAl-FSP catalyst.

To further elucidate the noble metal cluster formation/redispersion starting from the oxidized state, we investigated the oxidation and reduction rate of Pd during a gas atmosphere switching experiment. *Operando* XAS characterization was conducted at different temperatures between 60 and 100 °C while changing the reaction mixture every 90 s between the 1000 ppm CO/10% O_2/He, and 10% O_2/He atmosphere. As can be seen from the LCA results reported in Figure 2a–c, the catalyst gives a rapid response to the change in reactive atmosphere at each investigated temperature, being partially reduced in reaction mixture and reoxidized in oxygen atmosphere.

The Pd reduction observed in the lean reaction mixture underlines the strong reductive nature of CO at low temperatures, even at relatively low concentrations. As it can be further observed by the first derivative of the smoothed averaged fraction of oxidized Pd species given in Figure 2d–f, the oxidation and reduction rates significantly change with increasing temperature. At 63 °C (Figure 2d), the oxidation process proceeds faster than reduction. Conversely, both oxidation and reduction occur at comparable rates at 87 °C (Figure 2e). At 100 °C (Figure 2f), an even faster reduction rate of Pd is measured, which indicates possible sintering and the formation of larger Pd clusters under the reaction conditions. Hence, although the oxidation rate remains similar at the three investigated temperatures, a significant increase in the reduction rate is observed with higher temperatures. Furthermore, at 100 °C, a slight but continuous reduction of Pd species is observed during the consecutive redox cycles when comparing the initial (the fraction of Pd_{ox} ≈ 0.8) and final (Pd_{ox} ≈ 0.7) states of the noble metal under reaction

https://doi.org/10.1021/acscatal.4c02077
ACS Catal. 2024, 14, 14871–14886

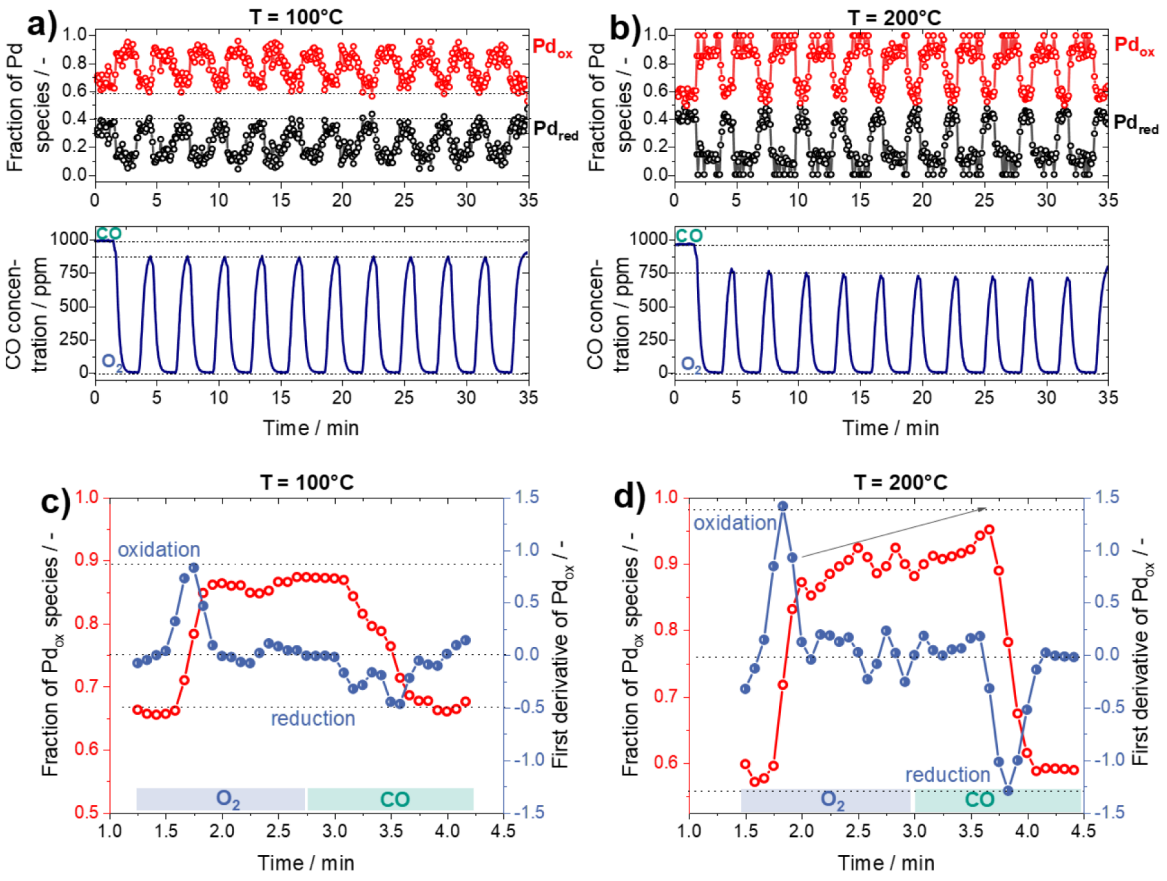

Figure 3. Linear combination results (LCA) of the Pd K-edge XANES spectra of 0.5Pd 5CeAl-FSP during cycling experiments between 1000 ppm CO/He and 10% O_2/He mixture at different temperatures (T = 100 and 200 °C) (a, b). The gas mixture was switched every 90 s during 11 cycles. The smoothed fraction of oxidized Pd species averaged over all cycles is additionally given for each temperature with the corresponding first derivative (c, d).

conditions. This behavior is in line with the data reported in Figure 1, and it corresponds to the formation of larger and more reduced Pd clusters. All in all, the variation in the redox response combined with the increase in Pd clusters seem to occur around the change in the CO oxidation activity profile (Figure 1a), evidencing two regions with different behaviors below and above approximately 90 °C.

In a next step, a slightly modified redox switching experiment was applied to the 0.5Pd 5CeAl-FSP catalyst at two different temperatures (100 and 200 °C). After heating in 1000 ppm CO to the desired temperature, the gas mixture was switched between 1000 ppm CO/He and 10% O_2/He every 90 s. In this way, we could differentiate between the effect of the reaction mixture and only CO on the Pd cluster formation. Starting with a partially reduced state for the noble metal (Pd_{ox} ≈ 0.7), a fast Pd reoxidation is observed at 100 °C when switching the gas mixture. However, Pd is not fully oxidized during the redox cycle (Pd_{ox} ≈ 0.9), despite the strong oxidizing conditions (Figure 3a,c). At 200 °C the switching experiment begins with a more pronounced redox response (Figure 3b,d) and a steep increase in the oxidation state of Pd. A further slow reoxidation of the noble metal is noticed over the time frame of the switching step, which indicates the bulk oxidation of the Pd clusters/nanoparticles (Figure 3d). The increase in the oxidation and reduction rates at higher temperatures is also in this case demonstrated by the first derivative curve at 200 °C in comparison to the one obtained at 100 °C (Figure 3c,d). Hence, the results of the redox cycling experiments furthermore underline the dynamics observed during the *operando* XAS measurements discussed above (Figure 1) and substantiate the reoxidation/redispersion of Pd clusters in lean reaction atmosphere at T > 100 °C.

3.2. Influence of Redispersion on Catalytic Performance. To gain insight into the redispersion process, which occurs at elevated temperatures under oxidizing conditions, ETEM measurements under model reaction conditions were performed. Despite the demonstration of dynamic changes of the noble metal state at high temperatures under oxidizing or reductive atmosphere for Pt/CeO_2 in previous studies,[22,71,72] these processes have not been addressed so far for Pd/CeO_2-based samples due to the poor contrast between Pd and CeO_2. To the best of our knowledge, mostly EDXS maps are used to identify the nature of the Pd species on CeO_2. In our ETEM study, a 1.0 wt % Pd catalyst supported on pure CeO_2 with a low surface area (LSA) of 35 m^2/g was selected. According to *ex situ* HAADF-STEM and EDXS characterization of the as-prepared catalyst, Pd is distributed across the CeO_2 support (Figure S4a). As expected, the relatively high concentration of Pd on CeO_2 facilitates the cluster formation under reaction conditions, leading to high oxidation activity at low temperatures (Figure S5b). Prior to the ETEM measurements, the catalyst was treated for 1 h in 10 mbar O_2 at 500 °C to remove the hydrocarbons and water molecules present on the surface. To induce the formation of metallic Pd nanoparticles, the sample was heated to 600 °C in 1.5 mbar H_2. This higher temperature (compared to the catalytic tests and *operando* XAS

https://doi.org/10.1021/acscatal.4c02077
ACS Catal. 2024, 14, 14871−14886

measurements above) was selected because of the significantly lower H_2 pressure during the ETEM measurements in comparison to the laboratory tests.

After approximately 1.5 h of reductive treatment, the formation of small Pd nanoparticles with a size of 1−2 nm was observed (Figure 4a), which remained stable after rapid

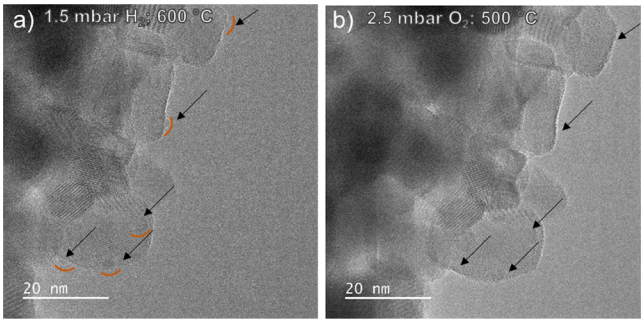

Figure 4. ETEM images of Pd/CeO_2-LSA acquired during *in situ* reduction (600 °C, 1.5 mbar H_2) and oxidation treatment (500 °C, 2.5 mbar O_2) revealing redispersion of Pd occurring at higher temperatures (500 °C) in 2.5 mbar O_2.

cooling (120 K/min) to room temperature in 1.5 mbar H_2 (Figure S18a). Afterward, the catalyst was treated in oxidizing atmosphere (2.5 mbar O_2) to initiate the redispersion of the previously formed Pd nanoparticles. As shown in Figure 4b, no Pd particles are visible after catalyst oxidation at 500 °C for 1 h, confirming the redispersion process. After cooling in 2.5 mbar O_2 (100 K/min), a final image of the redispersed catalyst state was taken at room temperature (Figure S18b). Redispersion of Pd on CeO_2 has also been reported in the literature, particularly after hydrothermal[73,74] or thermal[75,76] oxidizing treatments at temperatures above 500 °C. The influence of this noble metal dynamic behavior upon varying the gas atmosphere is shown by the activity profile obtained for the prereduced 1.0Pd/CeO_2-LSA catalyst during consecutive light-off/light-out cycles. While 50% of CO was converted already at 95 °C after catalyst activation by a short reductive treatment (5 min in 2% H_2/He at 200 °C), a pronounced decrease in the CO conversion was measured during the following activity cycles (T_{50} = 113 °C), as shown in Figure S19. In line with the ETEM results, this behavior is explained by the noble metal redispersion process that occurs at higher temperatures as soon as CO is converted at the beginning of the catalyst bed. Such catalyst deactivation via redispersion, occuring particularly at low noble metal loadings, was previously reported by Goodman et al.[77] for Pd/Al_2O_3 during CH_4 oxidation.

Overall, the revealed structural dynamics (sintering/redispersion) may also elucidate the hysteresis behavior observed for the 0.5Pd 5CeAl-FSP catalyst during the CO oxidation reaction. Such hysteresis describes the difference in activity during the light-off cycle compared to the light-out and is often attributed not only to thermal effects but also to the structural changes of the catalyst surface and bulk.[47,78−80] As visualized in Figure S7, a normal hysteresis behavior was observed for 0.5Pd 5CeAl-FSP during the first (degreening) catalytic run, with a higher catalytic performance being reached during the first light-out. By linking the observed activity with the *operando* XAS data discussed above (e.g., Figure 1), it can be concluded that the *in situ* formation of Pd clusters leads to the activity boost after the first light-off. On the contrary, an inverse hysteresis behavior was detected during the subsequent catalytic cycles. In this case, a lower catalytic performance during the light-out cycles can be attributed to the loss of active Pd clusters under oxidizing conditions at high temperatures. However, the formation of the Pd clusters is initiated again in the presence of CO during cooling, thus closing the catalyst lifecycle. This is in line with studies of Dubbe et al.[78] and Schalow et al.[81]

3.3. Effect of Catalyst Composition on Cluster Formation. To investigate the effect of the noble metal to CeO_2 weight ratio on the catalyst state and CO oxidation activity, a series of Pd/CeO_2−Al_2O_3 catalysts were prepared via double-nozzle flame spray pyrolysis. Analogously, Pd and CeO_2 precursors were sprayed separately from the alumina precursor solution to ensure a maximized Pd−CeO_2 interface (Figure S5a). The noble metal to CeO_2 ratio was varied in two ways: first, by changing the CeO_2 loading while keeping the Pd content the same (0.5 wt %) and second by adjusting the Pd content while the CeO_2 loading was set to 5.0 wt %.

According to the obtained activity results, which are shown in Figure 5, all synthesized catalysts show a promising catalytic performance with the temperature of 90% conversion below 150 °C. Compared to the activity shown by a reference Pd/Al_2O_3 catalyst with the reaction onset above 100 °C (Table S2), these catalytic trends encompass the role of the Pd−CeO_2 interface in addition to that of Pd clusters for obtaining a high CO oxidation activity in the low temperature region. However, as can be seen in Figure 5a, the increase of CeO_2 content has a negative impact on the CO oxidation activity at temperatures above 75 °C. Despite the three catalysts having an almost identical reaction onset until 75 °C, the sample with the highest CeO_2 content of 20% (green in Figure 5a) is the only one that did not reach full conversion below 150 °C. In contrast, the differences in activity above 75 °C between the 5% and 10% CeO_2 loaded samples are significantly less prominent (red and blue lines in Figure 5a). Only a slightly higher temperature is needed in the case of 0.5Pd 10CeAl-FSP to reach full CO conversion (ΔT_{100} = 15 K).

For the samples with various Pd loadings, a different trend can be seen in Figure 5b. During all catalytic tests, the amount of catalyst in the reactor was adjusted to the Pd loading to ensure comparability of the results. The sample with the highest Pd loading of 1.0%, (olive curve in Figure 5b) showed the lowest catalytic activity of the series. A higher CO oxidation rate was obtained for the 0.5Pd 5CeAl-FSP sample with a Pd:CeO_2 weight ratio of 1:10 (red curve, Figure 5b). A further decrease of the Pd content to 0.25% did not lead to additional activity improvement (gray curve in Figure 5b), in accordance with the results in the series reported in Figure 5a. Notably, the 0.25Pd 5CeAl-FSP and 0.5Pd 10CeAl-FSP catalysts with the same Pd:CeO_2 weight ratio of 1:20 show a very similar trend in CO conversion. Overall, the 0.5Pd 5CeAl-FSP sample seems to represent the optimum in terms of catalyst composition.

According to the XRD data, only the characteristic reflections of the support material (Al_2O_3 and CeO_2) were visible for all synthesized catalysts, indicating the presence of small Pd particles or dispersed Pd species (Figure S1). The results of the elemental analysis furthermore confirmed for all samples the desired Pd and CeO_2 loading and Pd:CeO_2 weight ratio. The *ex situ* XANES measurements showed that after calcination, Pd is present in the oxidation state +2 in all

https://doi.org/10.1021/acscatal.4c02077
ACS Catal. 2024, 14, 14871−14886

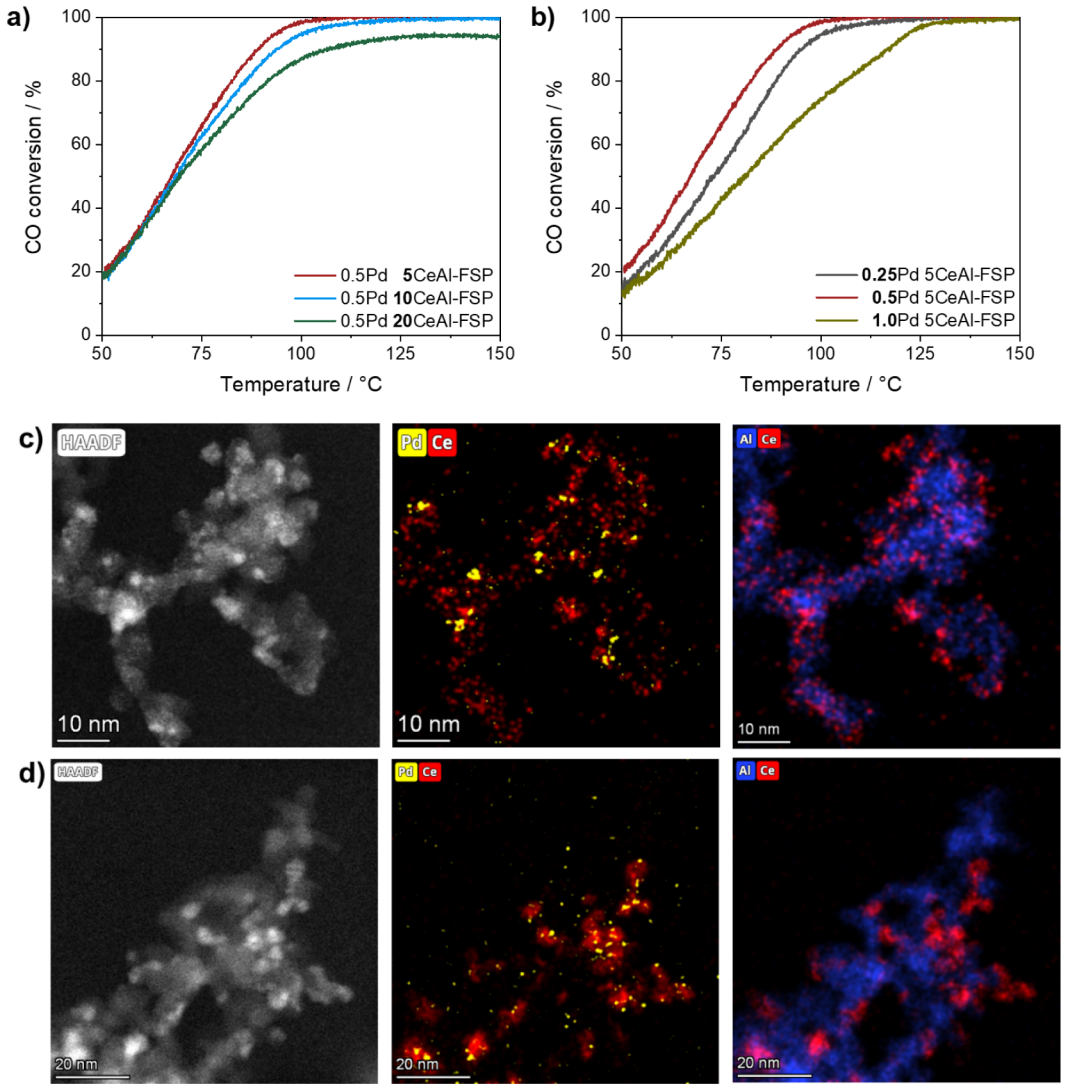

Figure 5. Catalytic activity results in terms of CO conversion of the FSP-synthesized Pd/CeO_2−Al_2O_3 catalysts during CO oxidation reaction (1000 ppm CO/8% O_2/N_2) after a degreening run showing the influence of CeO_2 (a) and Pd loading (b) (in all cases normalized to Pd amount, cf. experimental) on the catalytic performance. HAADF-STEM images with the corresponding EDXS mappings of 1.0Pd 5CeAl-FSP (c) and 0.5Pd 20CeAl-FSP (d).

samples (Figure S2). The noble metal state was further investigated by HAADF-STEM measurements for the catalysts with the highest CeO_2 content (0.5Pd 20CeAl-FSP) or Pd loading (1.0Pd 5CeAl-FSP), which represent two extreme cases in the range of synthesized catalysts. Again, the EDXS maps revealed the preferential location of Pd on the CeO_2 entities in both samples (Figure 5c,d), as also expected from the applied synthesis procedure with Pd and Ce precursors being sprayed in one flame. (Figure 5c,d). The comparison of the HAADF-STEM images and EDXS maps for these two samples furthermore underlines the influence of CeO_2 content on the size of CeO_2 and Pd entities. As expected, a higher CeO_2 loading of 20% resulted in the formation of larger CeO_2 islands on Al_2O_3. However, even in this case, CeO_2 particles have a size of below 10 nm (Figure 5d), which is in line with the applied synthesis method.

Based on these *ex situ* characterization results, a similar initial state was concluded for all catalysts. The differences in the catalytic performance allowed us to assume that there is an optimal size of Pd species for promoting the CO oxidation reaction at low temperatures. This size seems to depend on the Pd:CeO_2 weight ratio, which is the basis for noble metal cluster generation under the reaction conditions. The lower activity of the 1.0Pd 5CeAl-FSP and 0.5Pd 20CeAl-FSP samples may be caused by the formation of too large or too small Pd clusters or even by the inhibition of cluster formation.

3.4. Comparison of the Dynamics of Pd/CeO_2−Al_2O_3 Catalysts with Varying Pd and CeO_2 Loading. To be able to track the dynamic changes of the active sites during CO oxidation, the state of catalysts with varying Pd and CeO_2 content was evaluated using DRIFTS. The results of the DRIFTS measurements in the reaction mixture at different temperatures (30−110 °C) are shown in Figure 6. Generally, a pronounced influence of the noble metal to CeO_2 ratio is observed on the evolution of Pd species in reaction atmosphere. The DRIFTS spectra in Figure 6 are ordered according to the increasing CeO_2 content (panels a−c) or increasing Pd loading (panels d−f). The IR spectra of all investigated catalysts show two prominent bands at ∼2150 and 2115 cm^{-1}. Both bands can be assigned to Pd^{2+}−CO and

https://doi.org/10.1021/acscatal.4c02077
ACS Catal. 2024, 14, 14871−14886

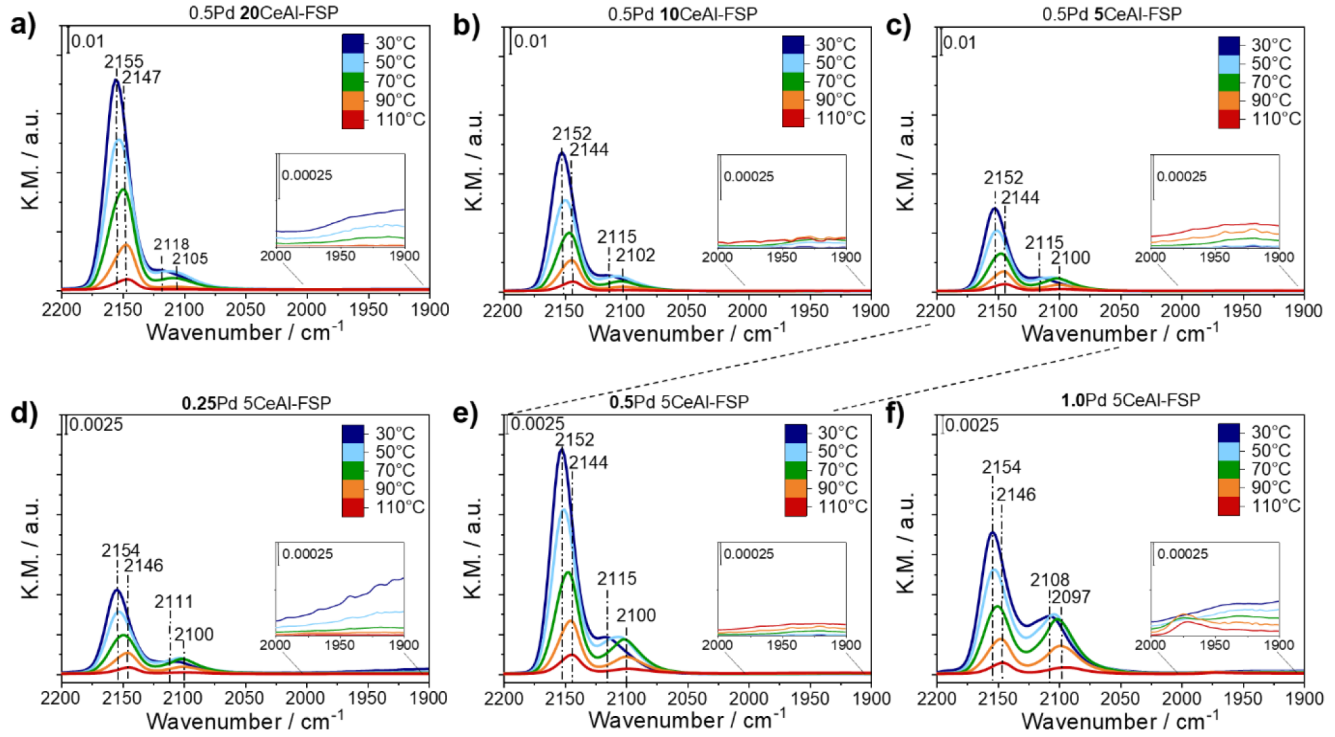

Figure 6. DRIFT spectra recorded after degreening run in 1000 ppm CO/10% O_2/He (200 mL/min) demonstrating the impact of increasing CeO_2 (a–c) and Pd (d–f) loading on species evolution under reaction conditions. Note that panel e represents the inset of panel c.

$Pd^{\delta+}$–CO, respectively,[25,66,82,83] which confirm the partial reduction of Pd species under reaction conditions. In line with the *operando* XAS measurements and similar to the Pt/CeO_2 system,[19,84] this step seems to be an important prerequisite for the high oxidation activity at low temperatures.

As can be seen in Figure 6a–c, the ratio of the two bands is directly influenced by the CeO_2 content. At higher CeO_2 loadings and therefore larger overall CeO_2 surface, the fraction of the IR band at ~2150 cm^{-1} increases significantly (Figure 6a). This band is often assigned to CO linearly adsorbed on the atomically dispersed Pd, and it indicates a higher dispersion degree of Pd atoms on CeO_2 in the 0.5Pd 20CeAl-FSP sample. In contrast, the band at ~2115 cm^{-1} becomes more prominent with higher Pd loadings. The DRIFTS spectrum obtained during CO adsorption on 1.0Pd 5CeAl-FSP (Figure 6f, right) clearly indicates the presence of a larger number of partially reduced Pd species in the sample. Keeping in mind the lower catalytic activity of the 1.0Pd 5CeAl-FSP catalyst in comparison to that of the 0.5Pd 5CeAl-FSP, we assume that the Pd:CeO_2 weight ratio of 1:5 promotes the formation of too large clusters/particles in the 1.0Pd 5CeAl-FSP catalyst.

Interestingly, no prominent IR bands were detected for all samples at temperatures below 70 °C in the range of 2050–1900 cm^{-1} that corresponds to CO adsorbed on metallic Pd sites.[24,38,66,82] This observation suggests an oxidized state for the active Pd clusters in this temperature range. However, during catalyst heating, a low intensity band appeared at 1970–1920 cm^{-1} in the DRIFT spectra of the 0.5Pd 5CeAl-FSP and 1.0Pd 5CeAl-FSP catalysts at 90 and 110 °C, respectively. In agreement with existing literature[24,66,82] and also more recent DFT calculations,[38] we assign the bands in this region to bridged CO adsorbed on metallic Pd (Pd_2^0–CO). For the 1.0Pd 5CeAl-FSP sample, the IR band was significantly more pronounced, which is in line with the higher probability of cluster/particle formation as obtained by increasing the Pd loading.

As underlined by the concept of surface noble metal concentration previously reported for Pt/CeO_2,[23] the results obtained in this study indicate as well that a higher noble metal loading or a smaller specific surface area of the support material increases the tendency to form noble metal clusters/particles. To further confirm this hypothesis for Pd/CeO_2-based catalysts, we have investigated the mobility of isolated Pd atoms on the CeO_2(111) surface, and therefore the probability of cluster formation, by DFT calculations. The diffusion energy diagram (Figure 7) shows that the energy

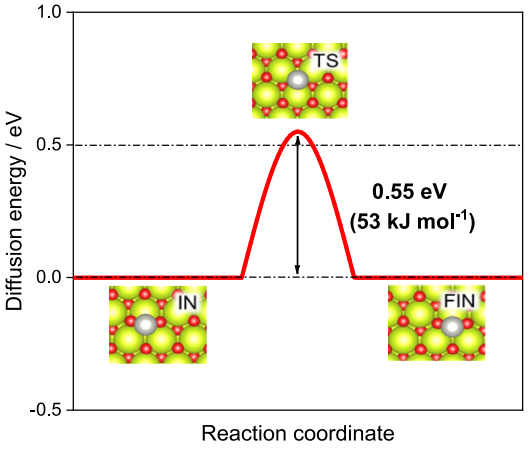

Figure 7. Diffusion energy diagram for a Pd single atom (gray circle solid, Pd) over 3 × 3 large unit cells of CeO_2(111) (yellow circle solids, Ce; red circle solid, O) and visualization of diffusion path with initial (IN), transition (TS), and final (FIN) state.

https://doi.org/10.1021/acscatal.4c02077
ACS Catal. 2024, 14, 14871–14886

barrier for a Pd single atom on the $CeO_2(111)$ surface is of the order of 0.55 eV (53 kJ mol^{-1}), which is lower in comparison to the similar diffusion process of a Pt single atom supported on $CeO_2(111)$ (90 kJ mol^{-1}).[23] This fact indicates a lower energy of interaction between the Pd atom and the oxygen of the CeO_2 surface in comparison to the $Pt/CeO_2(111)$ system. Therefore, we assume a facilitated cluster formation for the Pd/CeO_2 system with a higher surface noble metal concentration. In addition to the simple diffusion of a Pd atom across the $CeO_2(111)$ surface (Figure 7), we considered a system with two adsorbed Pd atoms and their diffusion and aggregation to form a Pd_2 cluster (Figure S20). This process is downhill in energy, as Pd_2 is more stable than a single Pd atom adsorbed on ceria. Likewise, the formation of $Pd_3/CeO_2(111)$ is also downhill relative to $Pd/CeO_2(111)$ and $Pd_2/CeO_2(111)$ (Figure S21). Additionally, diffusion barriers of $Pd_2/CeO_2(111)$ and $Pd_3/CeO_2(111)$ are given in Figures S22 and S23.

In order to validate the general applicability of the concept, the influence of the synthesis method on cluster formation and, therefore, on the catalytic performance was evaluated. For this purpose, catalysts with the same chemical composition as the 0.5Pd 5CeAl-FSP and 0.5Pd 10CeAl-FSP samples, which showed the most promising catalytic behavior, were prepared by incipient wetness impregnation (IWI). The results of the catalytic activity tests revealed similar CO conversion profiles, with the IWI-synthesized catalysts showing an even slightly better activity (Figure S6). The minor difference in activity might be caused by a slightly better availability of Pd on the catalyst surface after impregnation in comparison to that shown by the FSP-synthesized sample. Possible encapsulation of Pd into the support cannot be fully prevented during the FSP synthesis, which represents one of the main disadvantages of FSP.[85,86] Nevertheless, it should be noted that especially for a higher CeO_2 content, a better distribution of CeO_2 islands on Al_2O_3 can be reached via the FSP preparation method (Figure S3b,d). Moreover, the localization of Pd on CeO_2 is directly enforced during the FSP synthesis by spraying Pd and CeO_2 precursors in one flame. Therefore, these findings confirm that the activity does not depend on the applied synthesis method but seems to be mainly defined by the noble metal−ceria weight ratio, underlining the robustness of the used concept. In a broader perspective, this approach can be further applied for rational design of active and stable noble metal−ceria catalysts for other applications beyond CO oxidation, where noble metal clusters represent the active species.

Overall, we found that the Pd cluster formation tendency in a $Pd/CeO_2-Al_2O_3$ catalyst correlates with the noble metal loading relative to the ceria content/surface area, i.e., $Pd:CeO_2$ weight ratio, but not relative to the alumina surface area. This relationship is illustrated in the top part of Figure 8 that shows the T25, T50, and T90 values as a function of the noble metal to ceria weight ratio. Since the dynamic nature of Pd clusters in Pd/CeO_2-based catalysts makes it very challenging to estimate the exact number of the active surface sites under transient reaction conditions, no TOF values were used for the comparison between the samples in our study. However, when comparing it to the total amount of Pd in the catalyst, we obtain a reaction rate of 0.018 mol_{CO} $mol^{-1}{}_{Pd}$ s^{-1} at T25 (54 °C), which is higher than the activity reported in the literature for Pd/CeO_2 catalysts at comparable temperatures[25,74,83] and that of the 0.5% Pd/Al_2O_3 reference catalyst in our study (Table S14). Based on the obtained activity results, it seems

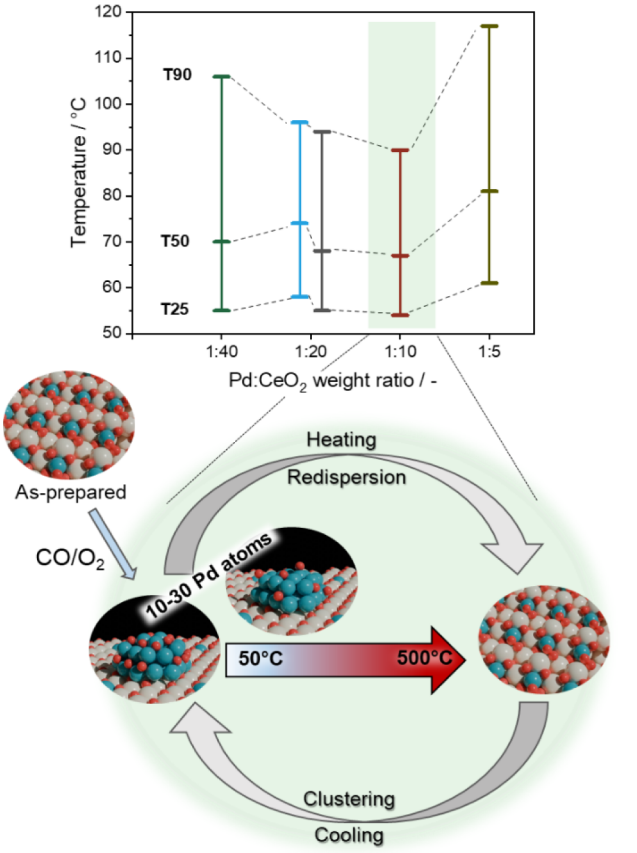

Figure 8. Light-off temperature of 25, 50, and 90% CO conversion (T25, T50, and T90) as a function of $Pd:CeO_2$ weight ratio showing a clear correlation between CO oxidation activity and chemical composition of the catalysts (top). Note that in all cases, the same amount of noble metal was loaded in the reactor. Schematic representation of dynamic structural changes of a $Pd/CeO_2-Al_2O_3$ catalyst (green circle solids, Pd; yellow circle solids, Ce; red circle solids, O) as a function of reaction mixture and temperature (bottom).

that the oxidized Pd clusters, containing few Pd atoms, are catalytically the most active species at lower temperatures, while larger, more reduced Pd nanoparticles become important for CO conversion at higher temperatures. Although the cluster formation rate under reaction conditions can be influenced by the chemical composition of the catalysts, the stability of the formed clusters distinctly depends on the reactive gas atmosphere and the temperature window of the investigated reaction.

The structural changes that occur in the $Pd/CeO_2-Al_2O_3$ catalyst over the catalytic cycle are also depicted in Figure 8 (bottom part). Despite the fact that a similar state is present in the as-prepared catalytic systems, the best CO oxidation activity was obtained for the 0.5Pd 5CeAl-FSP catalyst with the $Pd:CeO_2$ weight ratio of 1:10. For this catalyst, Pd clusters containing between 10 and 30 atoms (as estimated from EXAFS/DFT) are formed upon exposure to reaction mixture and catalyst degreening. During the light-off cycle, the clusters remain stable below 100 °C and are slowly oxidized/redispersed by O_2 starting from 100−150 °C when CO is fully converted. The reversible nature of the structural changes as a function of temperature and reaction conditions is also underlined by the *operando* XAS measurements during gas

https://doi.org/10.1021/acscatal.4c02077
ACS Catal. 2024, 14, 14871−14886

atmosphere switching experiments between reducing (CO/O_2 or CO) and oxidizing (O_2) conditions. In this regard, increasing the light-off temperature results in a more pronounced redox response of the noble metal. At higher temperatures and complete CO conversion (>300 °C), the noble metal redispersion process takes place due to the predominant oxidizing atmosphere along the catalyst bed and strong Pd−CeO_2 interaction, as revealed by *operando* XAS and ETEM measurements. *Operando* XAS data also show that while cooling in reaction mixture, the reductive nature of CO leads again to the formation of Pd clusters below 150 °C, closing the lifecycle of the catalyst. Hence, despite the noble metal−ceria systems being known to be very dynamic under reducing or oxidizing conditions at high temperatures, here, we show that even 1000 ppm CO is sufficient to initiate the *in situ* formation of active Pd clusters in Pd/CeO_2−Al_2O_3 materials at very low temperatures.

4. CONCLUSIONS

This study demonstrates that an understanding of the catalytic lifecycle of Pd entities in Pd/CeO_2−based catalysts by means of complementary *in situ/operando* characterization techniques is essential to explain the catalytic activity and unravel the nature of the most active species. The *operando* spectroscopic results together with the systematic variation of the Pd:CeO_2 ratio show that single Pd atoms are catalytically less active for CO oxidation. Therefore, the single site formation during CO oxidation should be prevented while the threshold of cluster formation should be enhanced, e.g., by use of mixed CeO_2−Al_2O_3 where ceria does not form composites with alumina and Pd is mainly located on ceria. According to our findings, the Pd to CeO_2 ratio is a key descriptor for Pd agglomeration under reaction conditions. However, the cluster formation rate strongly depends not only on the chemical composition of the catalyst but also on the applied reaction conditions, i.e., CO and O_2 concentration in the reaction mixture. Hence, these parameters should be considered during catalyst design and application. In our case, the highest activity during CO oxidation in a high excess of oxygen (lean conditions) was observed for the catalyst with the Pd to CeO_2 ratio of 1:10. The use of mixed CeO_2−Al_2O_3 supports allows to obtain an optimal cluster size range of 10−30 atoms and prevents strong sintering and redispersion under reaction conditions. Additionally, only a minimal effect of the preparation procedure was identified. This concept of rational triggering of the Pd agglomeration by tuning the Pd to CeO_2 ratio can be transferred to other catalytic systems and related applications, allowing the increase of the atomic efficiency of noble metal-based catalysts.

■ ASSOCIATED CONTENT

Data Availability Statement

The data that support the findings of this study are available in KITopen at https://doi.org/10.35097/0k5f6x56uxjsw7cw.

Supporting Information

The Supporting Information is available free of charge at https://pubs.acs.org/doi/10.1021/acscatal.4c02077.

Ex situ characterization, catalytic activity, and DRIFTS data; EXAFS data analysis including used structural models as well as time-resolved XANES data recorded during MES experiments; agglomeration/diffusion energy diagrams received by DFT investigations (PDF)

■ AUTHOR INFORMATION

Corresponding Author

Jan-Dierk Grunwaldt − *Institute for Chemical Technology and Polymer Chemistry (ITCP), Karlsruhe Institute of Technology (KIT), Karlsruhe 76131, Germany; Institute of Catalysis Research and Technology (IKFT), Karlsruhe Institute of Technology (KIT), Eggenstein-Leopoldshafen 76344, Germany;* orcid.org/0000-0003-3606-0956; Email: grunwaldt@kit.edu

Authors

Daria Gashnikova − *Institute for Chemical Technology and Polymer Chemistry (ITCP), Karlsruhe Institute of Technology (KIT), Karlsruhe 76131, Germany*

Florian Maurer − *Institute for Chemical Technology and Polymer Chemistry (ITCP), Karlsruhe Institute of Technology (KIT), Karlsruhe 76131, Germany;* orcid.org/0000-0002-3307-4132

Miriam R. Bauer − *Institute for Chemical Technology and Polymer Chemistry (ITCP), Karlsruhe Institute of Technology (KIT), Karlsruhe 76131, Germany*

Sarah Bernart − *Institute of Catalysis Research and Technology (IKFT), Karlsruhe Institute of Technology (KIT), Eggenstein-Leopoldshafen 76344, Germany*

Jelena Jelic − *Institute of Catalysis Research and Technology (IKFT), Karlsruhe Institute of Technology (KIT), Eggenstein-Leopoldshafen 76344, Germany*

Mads Lützen − *National Centre for Nano Fabrication and Characterization (DTU Nanolab), Technical University of Denmark (DTU), Lyngby 2800Kgs, Denmark*

Carina B. Maliakkal − *Institute of Nanotechnology (INT) and Karlsruhe Nano Micro Facility (KNMFi), Karlsruhe Institute of Technology (KIT), Eggenstein-Leopoldshafen 76344, Germany*

Paolo Dolcet − *Institute for Chemical Technology and Polymer Chemistry (ITCP), Karlsruhe Institute of Technology (KIT), Karlsruhe 76131, Germany; Department of Chemical Sciences, University of Padova, Padova 35131, Italy;* orcid.org/0000-0001-9583-9375

Felix Studt − *Institute for Chemical Technology and Polymer Chemistry (ITCP), Karlsruhe Institute of Technology (KIT), Karlsruhe 76131, Germany; Institute of Catalysis Research and Technology (IKFT), Karlsruhe Institute of Technology (KIT), Eggenstein-Leopoldshafen 76344, Germany;* orcid.org/0000-0001-6841-4232

Christian Kübel − *Institute of Nanotechnology (INT) and Karlsruhe Nano Micro Facility (KNMFi), Karlsruhe Institute of Technology (KIT), Eggenstein-Leopoldshafen 76344, Germany; Institute of Materials Research, Technical University Darmstadt (TUDa), Darmstadt 64287, Germany;* orcid.org/0000-0001-5701-4006

Christian D. Damsgaard − *National Centre for Nano Fabrication and Characterization (DTU Nanolab) and Department of Physics (DTU Physics), Technical University of Denmark (DTU), Lyngby 2800Kgs, Denmark;* orcid.org/0000-0002-3117-8616

Maria Casapu − *Institute for Chemical Technology and Polymer Chemistry (ITCP), Karlsruhe Institute of Technology (KIT), Karlsruhe 76131, Germany;* orcid.org/0000-0002-8755-9856

Complete contact information is available at: https://pubs.acs.org/10.1021/acscatal.4c02077

Notes

The authors declare no competing financial interest.

■ ACKNOWLEDGMENTS

D.G. acknowledges the "Fonds der Chemischen Industrie" (FCI) of the Verband der Chemischen Industrie e.V. (VCI) for financial support during her Ph.D. studies. This study and her work were further funded by the Deutsche Forschungsgemeinschaft (DFG, German Research Foundation) − SFB 1441 − project ID 426888090 (projects A3/B1, B2, B3, and B4). The authors acknowledge the synchrotron radiation facility SOLEIL for beamtime at the ROCK and SAMBA beamlines (Saint-Aubin, France) as well as both beamline teams for their assistance during operando XAS experiments. This work was supported by a public grant overseen by the French National Research Agency (ANR) as part of the "Investissements d'Avenir" program (reference: ANR-10-EQPX-45). The authors further thank the KIT light source for beamtime at the CAT-ACT beamline and A. Zimina (IKFT, KIT) for performing *ex situ* measurements. Additionally, E. Welter and R. Biller are acknowledged for assistance in using the photon beamline P65 at DESY (Hamburg, Germany). The authors also thank M. Stehle and S.-L. Heck (ITCP, KIT) for their help during the *operando* XAS experiments. Electron microscopy was supported by the Karlsruhe Nano Micro Facility (KNMFi), a Helmholtz Research Infrastructure at KIT. The authors thank D. Wang for discussion of STEM results. T. Bergfeldt (IAM-AWP, KIT) is acknowledged for ICP-OES analysis and M. Makowiak (IKFT, KIT) for BET measurements. N. Küstner is acknowledged for his commitment during pupil internship and assistance in the catalyst preparation. M.L. and C.D.D. acknowledge support from the VILLUM FONDEN research grant (9455). The authors acknowledge support by the state of Baden-Württemberg through bwHPC and the German Research Foundation (DFG) through grant no. INST 40/575-1 FUGG (JUSTUS2, RVs bw17D011). The authors thank DAPHNE4NFDI (DFG project under project number 460248799) as well as further NFDI-consortia (NFDI4Cat, FAIRMAT and NFDI4Chem) for fruitful discussion and valuable input for implementing FAIR data principles in this work.

■ REFERENCES

(1) Adijanto, L.; Sampath, A.; Yu, A. S.; Cargnello, M.; Fornasiero, P.; Gorte, R. J.; Vohs, J. M. Synthesis and stability of Pd@CeO_2 core−shell catalyst films in solid oxide fuel cell anodes. *ACS Catal.* **2013**, *3*, 1801−1809.

(2) Miller, H. A.; Bellini, M.; Dekel, D. R.; Vizza, F. Recent developments in Pd-CeO_2 nano-composite electrocatalysts for anodic reactions in anion exchange membrane fuel cells. *Electrochem. Commun.* **2022**, *135*, 107219.

(3) Liu, Y.; Wang, Q.; Zhang, J.; Ding, J.; Cheng, Y.; Wang, T.; Li, J.; Hu, F.; Yang, H. B.; Liu, B. Recent Advances in Carbon-Supported Noble-Metal Electrocatalysts for Hydrogen Evolution Reaction: Syntheses, Structures, and Properties. *Adv. Energy Mater.* **2022**, *12*, 2200928.

(4) Zhang, F.; Zhu, Y.; Lin, Q.; Zhang, L.; Zhang, X.; Wang, H. Noble-metal single-atoms in thermocatalysis, electrocatalysis, and photocatalysis. *Energy Environ. Sci.* **2021**, *14*, 2954−3009.

(5) Long, F.; Liu, W.; Jiang, X.; Zhai, Q.; Cao, X.; Jiang, J.; Xu, J. State-of-the-art technologies for biofuel production from triglycerides: A review. *Renewable Sustainable Energy Rev.* **2021**, *148*, 111269.

(6) Chu, S.; Wang, E.; Feng, F.; Zhang, C.; Jiang, J.; Zhang, Q.; Wang, F.; Bing, L.; Wang, G.; Han, D. A Review of Noble Metal Catalysts for Catalytic Removal of VOCs. *Catalysts* **2022**, *12*, 1543.

(7) Zhang, L.; Xue, L.; Lin, B.; Zhao, Q.; Wan, S.; Wang, Y.; Jia, H.; Xiong, H. Noble Metal Single-Atom Catalysts for the Catalytic Oxidation of Volatile Organic Compounds. *ChemSuschem* **2022**, *15*, No. e202102494.

(8) Liu, L.; Corma, A. Metal Catalysts for Heterogeneous Catalysis: From Single Atoms to Nanoclusters and Nanoparticles. *Chem. Rev.* **2018**, *118*, 4981−5079.

(9) Rood, S.; Eslava, S.; Manigrasso, A.; Bannister, C. Recent advances in gasoline three-way catalyst formulation: A review. *Proc. Inst. Mech. Eng., Part D* **2020**, *234*, 936−949.

(10) Vieira, L. H.; Rasteiro, L. F.; Santana, C. S.; Catuzo, G. L.; da Silva, A. H.; Assaf, J. M.; Assaf, E. M. Noble Metals in Recent Developments of Heterogeneous Catalysts for CO_2 Conversion Processes. *ChemCatchem* **2023**, *15*, No. e202300493.

(11) Sarma, B. B.; Maurer, F.; Doronkin, D. E.; Grunwaldt, J.-D. Design of Single-Atom Catalysts and Tracking Their Fate Using Operando and Advanced X-ray Spectroscopic Tools. *Chem. Rev.* **2023**, *123*, 379−444.

(12) Dessal, C.; Len, T.; Morfin, F.; Rousset, J.-L.; Aouine, M.; Afanasiev, P.; Piccolo, L. Dynamics of Single Pt Atoms on Alumina during CO Oxidation Monitored by Operando X-ray and Infrared Spectroscopies. *ACS Catal.* **2019**, *9*, 5752−5759.

(13) Li, C.-H.; Wu, J.; Getsoian, A. B.; Cavataio, G.; Jinschek, J. R. Direct Observation of Rhodium Aluminate ($RhAlO_x$) and Its Role in Deactivation and Regeneration of Rh/Al_2O_3 under Three-Way Catalyst Conditions. *Chem. Mater.* **2022**, *34*, 2123−2132.

(14) Lu, Y.; Thompson, C.; Kunwar, D.; Datye, A. K.; Karim, A. M. Origin of the High CO Oxidation Activity on CeO_2 Supported Pt Nanoparticles: Weaker Binding of CO or Facile Oxygen Transfer from the Support? *ChemCatchem* **2020**, *12*, 1726−1733.

(15) Chakraborty, D.; Smitshuysen, T. E. L.; Kakekhani, A.; Jespersen, S. P. F.; Banerjee, S.; Krabbe, A.; Hagen, N.; Silva, H.; Just, J.; Damsgaard, C. D.; Helveg, S.; Rappe, A. M.; Norskov, J. K.; Chorkendorff, I. Reversible Atomization and Nano-Clustering of Pt as a Strategy for Designing Ultra-Low-Metal-Loading Catalysts. *J. Phys. Chem. C* **2022**, *126*, 16194−16203.

(16) Gänzler, A. M.; Betz, B.; Baier-Stegmaier, S.; Belin, S.; Briois, V.; Votsmeier, M.; Casapu, M. Operando X-ray Absorption Spectroscopy Study During Conditioning of Pt-Based Catalysts and Its Implications for CO Oxidation. *J. Phys. Chem. C* **2020**, *124*, 20090−20100.

(17) Jones, J.; Xiong, H.; DeLariva, A. T.; Peterson, E. J.; Pham, H.; Challa, S. R.; Qi, G.; Oh, S.; Wiebenga, M. H.; Pereira Hernández, X. I.; Wang, Y.; Datye, A. K. Thermally stable single-atom platinum-on-ceria catalysts via atom trapping. *Science* **2016**, *353*, 150−154.

(18) Dolcet, P.; Maurer, F.; Casapu, M.; Grunwaldt, J.-D. Insights into the Structural Dynamics of Pt/CeO_2 Single-Site Catalysts during CO Oxidation. *Catalysts* **2021**, *11*, 617.

(19) Maurer, F.; Jelic, J.; Wang, J.; Gänzler, A.; Dolcet, P.; Wöll, C.; Wang, Y.; Studt, F.; Casapu, M.; Grunwaldt, J.-D. Tracking the formation, fate and consequence for catalytic activity of Pt single sites on CeO_2. *Nat. Catal.* **2020**, *3*, 824−833.

(20) Gatla, S.; Aubert, D.; Agostini, G.; Mathon, O.; Pascarelli, S.; Lunkenbein, T.; Willinger, M. G.; Kaper, H. Room-temperature CO oxidation catalyst: Low-temperature metal−support interaction between platinum nanoparticles and nanosized ceria. *ACS Catal.* **2016**, *6*, 6151−6155.

(21) Pereira-Hernández, X. I.; DeLariva, A.; Muravev, V.; Kunwar, D.; Xiong, H.; Sudduth, B.; Engelhard, M.; Kovarik, L.; Hensen, E. J.; Wang, Y.; Datye, A. K. Tuning Pt-CeO_2 interactions by high-temperature vapor-phase synthesis for improved reducibility of lattice oxygen. *Nat. Commun.* **2019**, *10*, 1358.

(22) Gänzler, A. M.; Casapu, M.; Vernoux, P.; Loridant, S.; Cadete Santos Aires, F. J.; Epicier, T.; Betz, B.; Hoyer, R.; Grunwaldt, J.-D. Tuning the structure of platinum particles on ceria in situ for enhancing the catalytic performance of exhaust gas catalysts. *Angew. Chem., Int. Ed.* **2017**, *56*, 13078−13082.

(23) Maurer, F.; Beck, A.; Jelic, J.; Wang, W.; Mangold, S.; Stehle, M.; Wang, D.; Dolcet, P.; Gänzler, A. M.; Kübel, C.; Studt, F.;

https://doi.org/10.1021/acscatal.4c02077
ACS Catal. 2024, 14, 14871−14886

Casapu, M.; Grunwaldt, J.-D. Surface Noble Metal Concentration on Ceria as a Key Descriptor for Efficient Catalytic CO Oxidation. *ACS Catal.* **2022**, *12*, 2473−2486.
(24) Spezzati, G.; Su, Y.; Hofmann, J. P.; Benavidez, A. D.; DeLariva, A. T.; McCabe, J.; Datye, A. K.; Hensen, E. J. Atomically dispersed Pd−O species on CeO_2 (111) as highly active sites for low-temperature CO oxidation. *ACS Catal.* **2017**, *7*, 6887−6891.
(25) Muravev, V.; Spezzati, G.; Su, Y.-Q.; Parastaev, A.; Chiang, F.-K.; Longo, A.; Escudero, C.; Kosinov, N.; Hensen, E. J. Interface dynamics of Pd−CeO_2 single-atom catalysts during CO oxidation. *Nat. Catal.* **2021**, *4*, 469−478.
(26) Jiang, D.; Wan, G.; García-Vargas, C. E.; Li, L.; Pereira-Hernández, X. I.; Wang, C.; Wang, Y. Elucidation of the Active Sites in Single-Atom Pd_1/CeO_2 Catalysts for Low-Temperature CO Oxidation. *ACS Catal.* **2020**, *10*, 11356−11364.
(27) Jeong, H.; Kwon, O.; Kim, B.-S.; Bae, J.; Shin, S.; Kim, H.-E.; Kim, J.; Lee, H. Highly durable metal ensemble catalysts with full dispersion for automotive applications beyond single-atom catalysts. *Nat. Catal.* **2020**, *3*, 368−375.
(28) Gulyaev, R.; Stadnichenko, A.; Slavinskaya, E.; Ivanova, A.; Koscheev, S.; Boronin, A. In situ preparation and investigation of Pd/CeO_2 catalysts for the low-temperature oxidation of CO. *Appl. Catal., A* **2012**, *439*, 41−50.
(29) Hinokuma, S.; Fujii, H.; Okamoto, M.; Ikeue, K.; Machida, M. Metallic Pd Nanoparticles Formed by Pd−O−Ce Interaction: A Reason for Sintering-Induced Activation for CO Oxidation. *Chem. Mater.* **2010**, *22*, 6183−6190.
(30) Resasco, J.; DeRita, L.; Dai, S.; Chada, J. P.; Xu, M.; Yan, X.; Finzel, J.; Hanukovich, S.; Hoffman, A. S.; Graham, G. W.; Bare, S. R.; Pan, X.; Christopher, P. Uniformity Is Key in Defining Structure−Function Relationships for Atomically Dispersed Metal Catalysts: The Case of Pt/CeO_2. *J. Am. Chem. Soc.* **2020**, *142*, 169−184.
(31) Muravev, V.; Parastaev, A.; van den Bosch, Y.; Ligt, B.; Claes, N.; Bals, S.; Kosinov, N.; Hensen, E. J. Size of cerium dioxide support nanocrystals dictates reactivity of highly dispersed palladium catalysts. *Science* **2023**, *380*, 1174−1179.
(32) Li, X.; Pereira-Hernández, X. I.; Chen, Y.; Xu, J.; Zhao, J.; Pao, C.-W.; Fang, C.-Y.; Zeng, J.; Wang, Y.; Gates, B. C.; Liu, J. Functional CeO_x nanoglues for robust atomically dispersed catalysts. *Nature* **2022**, *611*, 284−288.
(33) Xie, S.; Tan, W.; Wang, C.; Arandiyan, H.; Garbrecht, M.; Ma, L.; Ehrlich, S. N.; Xu, P.; Li, Y.; Zhang, Y.; Collier, S.; Deng, J.; Liu, F. Structure-activity relationship of Pt catalyst on engineered ceria-alumina support for CO oxidation. *J. Catal.* **2022**, *405*, 236−248.
(34) Bañares, M. A. Operando methodology: Combination of in situ spectroscopy and simultaneous activity measurements under catalytic reaction conditions. *Catal. Today* **2005**, *100*, 71−77.
(35) Weckhuysen, B. M. Determining the active site in a catalytic process: Operando spectroscopy is more than a buzzword. *Phys. Chem. Chem. Phys.* **2003**, *5*, 4351−4360.
(36) Grunwaldt, J.-D.; Caravati, M.; Hannemann, S.; Baiker, A. X-ray absorption spectroscopy under reaction conditions: Suitability of different reaction cells for combined catalyst characterization and time-resolved studies. *Phys. Chem. Chem. Phys.* **2004**, *6*, 3037−3047.
(37) Meunier, F. C. Pitfalls and benefits of in situ and operando diffuse reflectance FT-IR spectroscopy (DRIFTS) applied to catalytic reactions. *React. Chem. Eng.* **2016**, *1*, 134−141.
(38) Salcedo, A.; Zengel, D.; Maurer, F.; Casapu, M.; Grunwaldt, J.-D.; Michel, C.; Loffreda, D. Identifying the Structure of Supported Metal Catalysts Using Vibrational Fingerprints from Ab Initio Nanoscale Models. *Small* **2023**, *19*, 2300945.
(39) Hansen, T. W.; Wagner, J. B.; Dunin-Borkowski, R. E. Aberration corrected and monochromated environmental transmission electron microscopy: Challenges and prospects for materials science. *Mater. Sci. Technol.* **2010**, *26*, 1338−1344.
(40) Teoh, W. Y.; Amal, R.; Mädler, L. Flame spray pyrolysis: An enabling technology for nanoparticles design and fabrication. *Nanoscale* **2010**, *2*, 1324−1347.
(41) Minnermann, M.; Grossmann, H. K.; Pokhrel, S.; Thiel, K.; Hagelin-Weaver, H.; Bäumer, M.; Mädler, L. Double flame spray pyrolysis as a novel technique to synthesize alumina-supported cobalt Fischer−Tropsch catalysts. *Catal. Today* **2013**, *214*, 90−99.
(42) Høj, M.; Pham, D. K.; Brorson, M.; Mädler, L.; Jensen, A. D.; Grunwaldt, J.-D. Two-Nozzle Flame Spray Pyrolysis (FSP) Synthesis of CoMo/Al_2O_3 Hydrotreating Catalysts. *Catal. Lett.* **2013**, *143*, 386−394.
(43) Brunauer, S.; Emmett, P. H.; Teller, E. Adsorption of gases in multimolecular layers. *J. Am. Chem. Soc.* **1938**, *60*, 309−319.
(44) Zimina, A.; Dardenne, K.; Denecke, M.; Doronkin, D.; Huttel, E.; Lichtenberg, H.; Mangold, S.; Pruessmann, T.; Rothe, J.; Spangenberg, T.; et al. CAT-ACT—A new highly versatile x-ray spectroscopy beamline for catalysis and radionuclide science at the KIT synchrotron light facility ANKA. *Rev. Sci. Instrum.* **2017**, *88*, 113113.
(45) Briois, V.; La Fontaine, C.; Belin, S.; Barthe, L.; Moreno, T.; Pinty, V.; Carcy, A.; Girardot, R.; Fonda, E. ROCK: The new Quick-EXAFS beamline at SOLEIL. *J. Phys.: Conf. Ser.* **2016**, *712*, 012149.
(46) Grunwaldt, J.-D.; Beier, M.; Kimmerle, B.; Baiker, A.; Nachtegaal, M.; Griesebock, B.; Lützenkirchen-Hecht, D.; Stötzel, J.; Frahm, R. Structural changes of noble metal catalysts during ignition and extinction of the partial oxidation of methane studied by advanced QEXAFS techniques. *Phys. Chem. Chem. Phys.* **2009**, *11*, 8779−8789.
(47) Casapu, M.; Fischer, A.; Gänzler, A. M.; Popescu, R.; Crone, M.; Gerthsen, D.; Türk, M.; Grunwaldt, J.-D. Origin of the normal and inverse hysteresis behavior during CO oxidation over Pt/Al_2O_3. *ACS Catal.* **2017**, *7*, 343−355.
(48) Gänzler, A. M.; Casapu, M.; Boubnov, A.; Müller, O.; Conrad, S.; Lichtenberg, H.; Frahm, R.; Grunwaldt, J.-D. Operando spatially and time-resolved X-ray absorption spectroscopy and infrared thermography during oscillatory CO oxidation. *J. Catal.* **2015**, *328*, 216−224.
(49) La Fontaine, C.; Belin, S.; Barthe, L.; Roudenko, O.; Briois, V. ROCK: A Beamline Tailored for Catalysis and Energy-Related Materials from ms Time Resolution to μm Spatial Resolution. *Synchrotron Radiat. News* **2020**, *33*, 20−25.
(50) Lesage, C.; Devers, E.; Legens, C.; Fernandes, G.; Roudenko, O.; Briois, V. High pressure cell for edge jumping X-ray absorption spectroscopy: Applications to industrial liquid sulfidation of hydrotreatment catalysts. *Catal. Today* **2019**, *336*, 63−73.
(51) Ravel, B.; Newville, M. ATHENA, ARTEMIS, HEPHAESTUS: Data analysis for X-ray absorption spectroscopy using IFEFFIT. *J. Synchrotron Radiat.* **2005**, *12*, 537−541.
(52) Ravel, B. Path aggregation techniques for EXAFS visualization and analysis. *J. Phys.: Conf. Ser.* **2013**, *430*, 012006.
(53) Newville, M. Larch: An analysis package for XAFS and related spectroscopies. *J. Phys.: Conf. Ser.* **2013**, *430*, 012007.
(54) Meunier, F. C. The design and testing of kinetically-appropriate operando spectroscopic cells for investigating heterogeneous catalytic reactions. *Chem. Soc. Rev.* **2010**, *39*, 4602−4614.
(55) Kresse, G.; Furthmüller, J. Efficient iterative schemes for ab initio total-energy calculations using a plane-wave basis set. *Phys. Rev. B* **1996**, *54*, 11169.
(56) Kresse, G.; Furthmüller, J. Efficiency of ab-initio total energy calculations for metals and semiconductors using a plane-wave basis set. *Comput. Mater. Sci.* **1996**, *6*, 15−50.
(57) Bahn, S. R.; Jacobsen, K. W. An object-oriented scripting interface to a legacy electronic structure code. *Comput. Sci. Eng.* **2002**, *4*, 56−66.
(58) Blöchl, P. E. Projector augmented-wave method, *Phys. Rev. B* **1994**, *50*, 17953.
(59) Kresse, G.; Joubert, D. From ultrasoft pseudopotentials to the projector augmented-wave method, *Phys. Rev. B* **1999**, *59*, 1758.
(60) Wellendorff, J.; Lundgaard, K. T.; Møgelhøj, A.; Petzold, V.; Landis, D. D.; Nørskov, J. K.; Bligaard, T.; Jacobsen, K. W. Density functionals for surface science: Exchange-correlation model development with Bayesian error estimation. *Phys. Rev. B* **2012**, *85*, 235149.

https://doi.org/10.1021/acscatal.4c02077
ACS Catal. 2024, 14, 14871−14886

(61) Dudarev, S. L.; Botton, G. A.; Savrasov, S. Y.; Humphreys, C.; Sutton, A. P. Electron-energy-loss spectra and the structural stability of nickel oxide: An LSDA+ U study. *Phys. Rev. B* **1998**, *57*, 1505.
(62) Monkhorst, H. J.; Pack, J. D. Special points for Brillouin-zone integrations. *Phys. Rev. B* **1976**, *13*, 5188.
(63) Henkelman, G.; Jónsson, H. Improved tangent estimate in the nudged elastic band method for finding minimum energy paths and saddle points. *J. Chem. Phys.* **2000**, *113*, 9978−9985.
(64) Henkelman, G.; Uberuaga, B. P.; Jónsson, H. A climbing image nudged elastic band method for finding saddle points and minimum energy paths. *J. Chem. Phys.* **2000**, *113*, 9901−9904.
(65) Gänzler, A. M.; Casapu, M.; Maurer, F.; Störmer, H.; Gerthsen, D.; Ferré, G. R.; Vernoux, P.; Bornmann, B.; Frahm, R.; Murzin, V.; Nachtegaal, M.; Votsmeier, M.; Grunwaldt, J.-D. Tuning the Pt/CeO_2 interface by in situ variation of the Pt particle size. *ACS Catal.* **2018**, *8*, 4800−4811.
(66) Muravev, V.; Simons, J. F.; Parastaev, A.; Verheijen, M. A.; Struijs, J. J.; Kosinov, N.; Hensen, E. J. Operando spectroscopy unveils the catalytic role of different palladium oxidation states in CO oxidation on Pd/CeO_2 catalysts. *Angew. Chem., Int. Ed.* **2022**, *61*, No. e202200434.
(67) Gänzler, A. M.; Casapu, M.; Doronkin, D. E.; Maurer, F.; Lott, P.; Glatzel, P.; Votsmeier, M.; Deutschmann, O.; Grunwaldt, J.-D. Unravelling the Different Reaction Pathways for Low Temperature CO Oxidation on Pt/CeO_2 and Pt/Al_2O_3 by Spatially Resolved Structure−Activity Correlations. *J. Phys. Chem. Lett.* **2019**, *10*, 7698−7705.
(68) Schalow, T.; Brandt, B.; Starr, D. E.; Laurin, M.; Shaikhutdinov, S. K.; Schauermann, S.; Libuda, J.; Freund, H.-J. Size-Dependent Oxidation Mechanism of Supported Pd Nanoparticles. *Angew. Chem., Int. Ed.* **2006**, *45*, 3693−3697.
(69) Ferré, G.; Aouine, M.; Bosselet, F.; Burel, L.; Cadete Santos Aires, F. J.; Geantet, C.; Ntais, S.; Maurer, F.; Casapu, M.; Grunwaldt, J.-D.; et al. Exploiting the dynamic properties of Pt on ceria for low-temperature CO oxidation. *Catal. Sci. Technol.* **2020**, *10*, 3904−3917.
(70) Nagai, Y.; Dohmae, K.; Ikeda, Y.; Takagi, N.; Tanabe, T.; Hara, N.; Guilera, G.; Pascarelli, S.; Newton, M. A.; Kuno, O.; Jiang, H.; Shinjoh, H.; Matsumoto, S. i. In Situ Redispersion of Platinum Autoexhaust Catalysts: An On-Line Approach to Increasing Catalyst Lifetimes? *Angew. Chem., Int. Ed.* **2008**, *47*, 9303−9306.
(71) Li, G.; Zakharov, D. N.; Hu, T.; Yu, Y.; Waluyo, I.; Hunt, A.; Head, A. R.; Boscoboinik, J. A. Tracking the dynamics of catalytic Pt/CeO_2 active sites during water-gas-shift reaction. *Commun. Mater.* **2024**, *5*, 133.
(72) Vincent, J. L.; Crozier, P. A. Atomic level fluxional behavior and activity of CeO2-supported Pt catalysts for CO oxidation. *Nat. Commun.* **2021**, *12*, 5789.
(73) Choi, M. S.; Jeong, H.; Lee, H. Re-dispersion of Pd-based bimetallic catalysts by hydrothermal treatment for CO oxidation. *RSC Adv.* **2021**, *11*, 3104−3109.
(74) Jeong, H.; Bae, J.; Han, J. W.; Lee, H. Promoting Effects of Hydrothermal Treatment on the Activity and Durability of Pd/CeO_2 Catalysts for CO Oxidation. *ACS Catal.* **2017**, *7*, 7097−7105.
(75) Hill, A. J.; Fisher, G. B.; Lenert, A.; Schwank, J. W. Intermediate temperature exposure regenerates performance and active site dispersion in sintered $Pd−CeO_2$ catalysts. *J. Catal.* **2022**, *415*, 186−199.
(76) Ye, J.; Xia, Y.; Cheng, D.-G.; Chen, F.; Zhan, X. Promoting effects of pretreatment on Pd/CeO2 catalysts for CO oxidation. *Int. J. Hydrogen Energy* **2019**, *44*, 17985−17994.
(77) Goodman, E. D.; Johnston-Peck, A. C.; Dietze, E. M.; Wrasman, C. J.; Hoffman, A. S.; Abild-Pedersen, F.; Bare, S. R.; Plessow, P. N.; Cargnello, M. Catalyst deactivation via decomposition into single atoms and the role of metal loading. *Nat. Catal.* **2019**, *2*, 748−755.
(78) Dubbe, H.; Eigenberger, G.; Nieken, U. Hysteresis phenomena on Pt-and Pd-diesel oxidation catalysts: Experimental observations. *Top. Catal.* **2016**, *59*, 1054−1058.
(79) Abedi, A.; Hayes, R.; Votsmeier, M.; Epling, W. S. Inverse hysteresis phenomena during CO and C_3H_6 oxidation over a Pt/Al_2O_3 catalyst. *Catal. Lett.* **2012**, *142*, 930−935.
(80) Lashina, E.; Slavinskaya, E.; Chumakova, N.; Stadnichenko, A.; Salanov, A.; Chumakov, G.; Boronin, A. Inverse temperature hysteresis and self-sustained oscillations in CO oxidation over Pd at elevated pressures of reaction mixture: Experiment and mathematical modeling. *Chem. Eng. Sci.* **2020**, *212*, 115312.
(81) Schalow, T.; Brandt, B.; Laurin, M.; Schauermann, S.; Libuda, J.; Freund, H.-J. CO oxidation on partially oxidized Pd nanoparticles. *J. Catal.* **2006**, *242*, 58−70.
(82) Sarma, B. B.; Jelic, J.; Neukum, D.; Doronkin, D. E.; Huang, X.; Studt, F.; Grunwaldt, J.-D. Tracking and Understanding Dynamics of Atoms and Clusters of Late Transition Metals with In-Situ DRIFT and XAS Spectroscopy Assisted by DFT. *J. Phys. Chem. C* **2023**, *127*, 3032−3046.
(83) Spezzati, G.; Benavidez, A. D.; DeLariva, A. T.; Su, Y.; Hofmann, J. P.; Asahina, S.; Olivier, E. J.; Neethling, J. H.; Miller, J. T.; Datye, A. K.; Hensen, E. J. M. CO oxidation by Pd supported on CeO_2 (100) and CeO_2 (111) facets. *Appl. Catal., B* **2019**, *243*, 36−46.
(84) Kunwar, D.; Zhou, S.; DeLariva, A.; Peterson, E. J.; Xiong, H.; Pereira-Hernández, X. I.; Purdy, S. C.; Ter Veen, R.; Brongersma, H. H.; Miller, J. T.; Hashiguchi, H.; Kovarik, L.; Lin, S.; Guo, H.; Wang, Y.; Datye, A. K. Stabilizing High Metal Loadings of Thermally Stable Platinum Single Atoms on an Industrial Catalyst Support. *ACS Catal.* **2019**, *9*, 3978−3990.
(85) van Vegten, N.; Maciejewski, M.; Krumeich, F.; Baiker, A. Structural properties, redox behaviour and methane combustion activity of differently supported flame-made Pd catalysts. *Appl. Catal., B* **2009**, *93*, 38−49.
(86) Pineau, N. J.; Keller, S. D.; Güntner, A. T.; Pratsinis, S. E. Palladium embedded in SnO_2 enhances the sensitivity of flame-made chemoresistive gas sensors. *Microchim. Acta* **2020**, *187*, 96.

https://doi.org/10.1021/acscatal.4c02077
ACS Catal. 2024, 14, 14871−14886